Title

Large Library Docking for Polypharmacology

Journal

Journal of Medicinal Chemistry, 69(5)

ISSN

0022-2623

Authors

Wu, Yujin
Vigneron, Seth
Braz, Joao
et al.

Publication Date

2026-03-12

DOI

10.1021/acs.jmedchem.5c03810

Peer reviewed

Journal of Medicinal Chemistry

pubs.acs.org/jmc

Article

Large Library Docking for Polypharmacology

Yujin Wu,[†] Seth Vigneron,[†] Joao Braz,[†] Karthik Srinivasan,[†] Elissa A. Fink, Xi-Ping Huang, Xinyu Xu, Harald Huebner, Joseph Y. Kim, Jing Wang, Tara Pfeiffer, Kensuke Sakamoto, Dmytro S. Radchenko, Ramona M. Rodriguiz, Yurii S. Moroz, John J. Irwin, Peter Gmeiner, Christian Billesboelle,* Bryan L. Roth,* Allan I. Basbaum,* Aashish Manglik,* William C. Wetsel,* and Brian K. Shoichet*

Cite This: *J. Med. Chem.* 2026, 69, 6210−6229

Read Online

ACCESS | Metrics & More | Article Recommendations | Supporting Information

ABSTRACT: Polypharmacological molecules are attractive for complex illnesses. Here, we explored large library docking for joint activity against target pairs. Retrospectively, as libraries grew, so too did the number of likely dual-activity molecules. In prospective docking of a 900-million molecule library against three target pairs (α_{2A}/SERT, MOR/SERT, and α_{2A}/MOR), we sought analgesic compounds. Both the α_{2A}/SERT and SERT/MOR campaigns led to dual binders with low μM to high nM activities with high hit rates; tetrahydropyridines from the α_{2A}/SERT campaign were also active against 5-HT$_{2A}$. However, even though cryo-EM structures confirmed the docking-predicted poses, optimization struggled to improve potency. Still, in mouse behavioral assays, the most potent α_{2A}/SERT compound (‘**z7149**) was effective against pain without inducing conditioned place preference, and the molecule had potent antidepression and anxiolytic drug-like behavior, consistent with its SERT/5-HT$_{2A}$ activities. This study reveals both advantages and challenges of docking for polypharmacology.

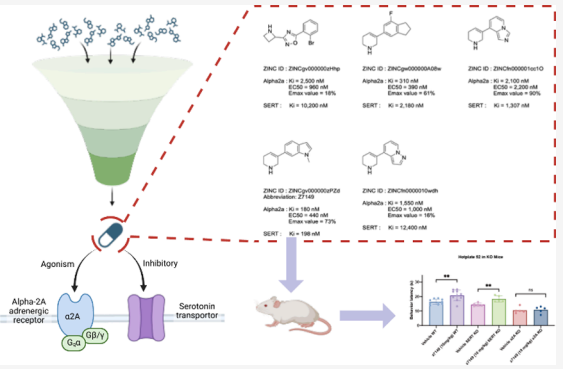

INTRODUCTION

Many diseases involve multiple proteins as primary drivers, and these may be targeted jointly for improved efficacy. Adequate treatment of blood pressure, for example, often combines drugs acting on calcium channels with those active on GPCRs (e.g., the angiotensin, the β_2- and α_2-adrenergic receptors), and with drugs acting on the angiotensin converting enzyme (ACE). In cancer treatment, kinase inhibitors and drugs targeting DNA replication and repair are frequently combined, while anti-inflammatory drugs acting on cyclooxygenases are often used in conjunction with μ-opioid receptor (MOR) agonists for pain. Against bacterial infection, drugs targeting different steps of the nucleoside biosynthesis pathway, (e.g., sulfa drugs and trimethoprim), as well as combinations like aminoglycosides and β-lactams, can act synergistically. These drugs are typically combined in fixed-dose combinations to improve therapeutic effects, safety, or compliance.[1−3] Challenges with this polypharmacy approach include differing pharmacokinetics of the individual drugs, more complicated coformulation, and drug−drug interactions.[1,2] μ

The liabilities with polypharmacy have motivated investigators to explore polypharmacology, where a single molecule simultaneously modulates multiple targets.[4] Polypharmacology is well-known among effective medications, including molecules like the antipsychotic clozapine, which acts against both the D$_2$ dopamine receptor for treating positive symptoms of schizophrenia and against the 5-HT$_{2A}$ serotonin receptor for countering the movement disorders induced by pure D$_2$-family antagonists, like chlorpromazine or haloperidol.[5] Similarly, triple reuptake inhibitors like LPM580098[6,7] have been developed for neuropathic pain due to their greater efficacy versus selective reuptake inhibitors. At a molecular level, pathway analysis has illuminated the mechanisms by which drugs active against multiple points in kinase cascades can have greater efficacy and reduced toxicity.[8,9] Similarly, the activity of tirzepatide at both GIP and GLP-1 receptors[10−12] may improve efficacy against obesity and type 2 diabetes; this area is among the most active foci for intentional GPCR polypharmacology. Still, apart from several proof-of-concept studies,[8,13] few polypharmacological drugs have been designed *de novo*; rather, multitarget actions have been revealed only after the drugs were approved.[14−20]

Several methods have been introduced to intentionally design or discover multitarget ligands, including ligand-based approaches, behavior-based screening,[4,21−33] and structure-based design.[13,24] For library docking, the focus of this study, results

Received: December 26, 2025
Revised: February 5, 2026
Accepted: February 11, 2026
Published: February 19, 2026

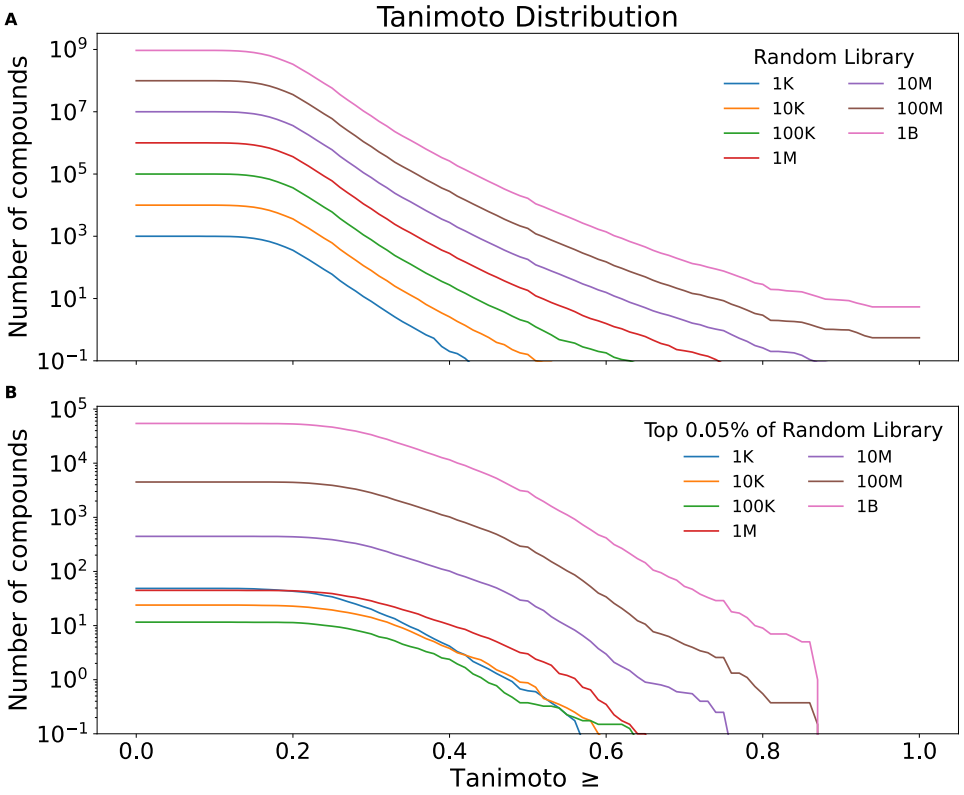

Figure 1. Similarity of library compounds and docking hits to known dual-target ligands as a function of library size. (A) The number of compounds resembling known joint D_2 and 5-HT_{2A} ligands as the library grows, measured by the maximum Tanimoto coefficient (Tc) between the molecules. (B) The number of compounds that resemble known joint D_2 and 5-HT_{2A} ligands by Tc values within the top 0.05% of the docking hit-lists for each receptor as the library grows. To be counted, the same molecule must appear in both hit lists.

have been mixed. While there have been examples of docking screens for molecules that intentionally modulate multiple targets,[23,25,28,29] affinities for these multiple targets have often been modest, or only highly related targets have been hit. Meanwhile, finding not only joint ligands but also those with the correct functions, such as agonists or antagonists, has been hit-and-miss. Though we ourselves have successfully found molecules that jointly target two receptors, the targets have typically been related (e.g., the dopamine D_2 and serotonin 5-HT_{2A} receptors, and the μ- and k-opioid receptors),[34,35] we have struggled to find ligands with the intended function[34,35] and the polypharmacology has often tracked with promiscuity.[34] In both a study seeking joint antagonists of the D_2 and 5-HT_{2A} receptor,[34] and one seeking agonist/antagonists against the μ- and k-opioid receptors,[35] we worried that the million-scale libraries being docked might be insufficient to sample ligands supporting selective polypharmacology.

Here we first investigated the impact of library growth on the docking-based discovery of dual target ligands. In retrospective studies, we examine the impact of such growth on the ability to dock for known and close-to-known polypharmacology ligands in libraries of increasing size. These studies supported prospective docking campaigns to find ligands that jointly targeted target pairs from different protein families, including the α_{2A} adrenergic receptor, a GPCR, together with the serotonin transporter SERT, and SERT with the MOR (a GPCR) for their combined utility for pain. Next we use predictions from these campaigns to experimentally test for joint activity on the paired targets. Further, we examine the overall hit-rates emerging from these studies along with our ability to optimize the polypharmacological ligands for potency and for pharmacokinetics. Finally, we examine the fidelity of the experimental structures of the ligands to their predicted geometries, and their in vivo activity as nonreinforcing analgesics, antidepressants, and anxiolytics. Both the opportunities and the substantial challenges of this approach are considered.

RESULTS

Retrospective Ligand Enrichment for Known Polypharmacology Targets

We begin with pairs of receptors known to share ligands for which structures are available and for which we have had success in docking to as individual targets.[34,36−39] Three target pairs were chosen: the D2 dopamine receptor (D_2) with the 5-HT_{2A} serotonin (5-HT, 5-hydroxytryptamine) receptor; the μ-opioid receptor (MOR) with the κ-opioid receptor (KOR); and the serotonin transporter (SERT) with the dopamine transporter (DAT).

We first asked how the number of likely dual-target ligands (SI file) increases with library size for the three target pairs, using similarity to known dual-target ligands as a metric. Using the D_2 and 5-HT_{2A} pair as an example, we identified 177 known ligands with affinities better than 1 μM for both targets from the ChEMBL database and calculated their similarity to 3 billion compounds in ZINC22[40] using ECFP4 topological fingerprints and Tanimoto coefficients (Tcs) to measure similarity. To evaluate the impact of the library growth, we randomly selected subsets of the 3 billion, from 1000 to 10,000··· to 1 billion compounds, over 100 times and plotted the similarity

https://doi.org/10.1021/acs.jmedchem.5c03810
J. Med. Chem. 2026, 69, 6210−6229

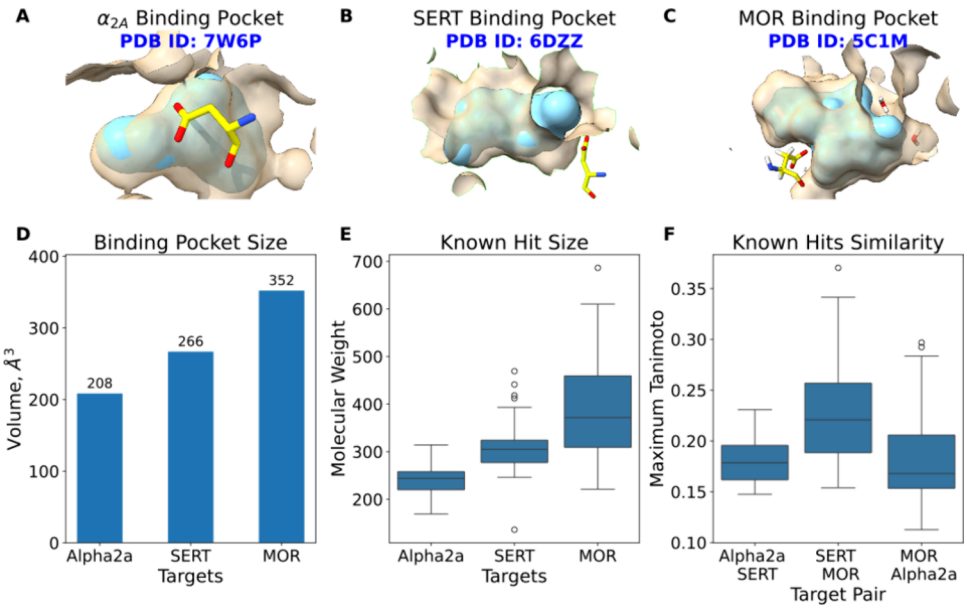

Figure 2. The physical characteristics of the three orthosteric pockets. (A) α_{2A} (PDB ID: 7W6P), (B) SERT (PDB ID: 6DZZ) and (C) MOR (PDB ID: 5C1M). Distribution of (D) binding pocket size, (E) molecular weight of known hits, and (F) their similarities.

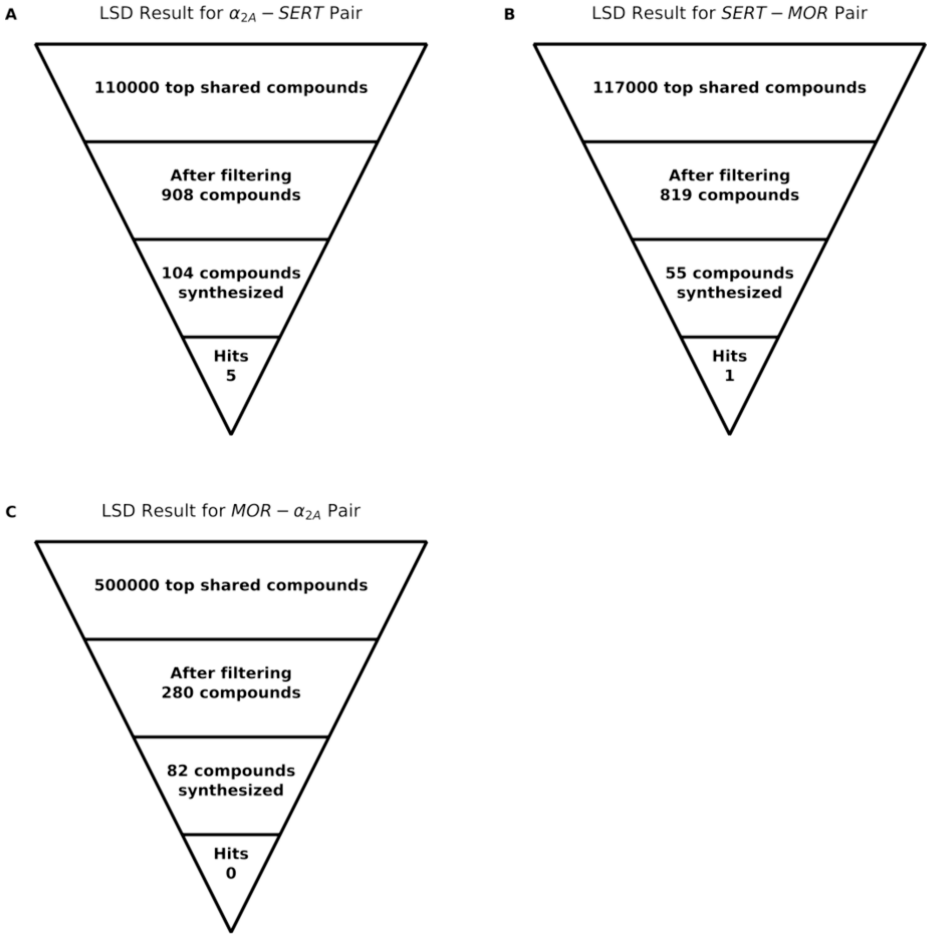

Figure 3. Summary of large-scale docking (LSD) results for dual target (A) α_{2A} and SERT, (B) SERT and MOR, and (C) MOR and α_{2A}. The postprocessing filtering steps include filtering based on molecular internal strain energy, key interactions with receptor residues and clustering based on pairwise similarity.[36−39,48,58]

https://doi.org/10.1021/acs.jmedchem.5c03810
J. Med. Chem. 2026, 69, 6210−6229

distributions. As library grew, the likelihood of finding molecules similar to the known dual-target compounds also grew (Figure 1A; SI Figure 1).

Having found that the number of likely dual target ligands grew with the library, we next asked whether docking can enrich these ligands and close analogs relative to the rest of the library, which we treated as nonbinders. We randomly selected libraries of increasing size from ZINC22[40] and docked them against D_2 and 5-HT_{2A}, using docking parameters used in previous studies against these targets.[38,41] We harvested the top 0.05% molecules by docking score and identified compounds that appeared in both lists. As the library grew so too did the likelihood that docking would find molecules that resemble known polypharmacological ligands among the top ranking 0.05% molecules for a target, counting only those that were shared between the two receptors (Figure 1B). By the time a billion molecules had been reached, docking found hundreds of likely polypharmacological molecules among the top ranked (SI Figures 2−4).

Prospective Discovery of Novel Polypharmacological Agonists

Encouraged by the retrospective results, we selected three biologically relevant but structurally distinct targets known for their role in pain or antidepressant-like action: the alpha-2A adrenergic receptor (α_{2A}), the serotonin transporter (SERT), and the μ-opioid receptor (MOR). Both α_{2A} and MOR agonists are well-known to confer analgesia[37,42−48] and their effects can synergize when coadministered.[49−51] Meanwhile, SERT inhibitors have been considered as treatments for chronic and neuropathic pain,[52−55,55−57] though their efficacy when used alone is often modest. Here we sought molecules that could: (1) activate both α_{2A} and inhibit SERT; (2) activate MOR and inhibit SERT; or (3) jointly activate α_{2A} and MOR. Our strategy, as in the retrospective calculations, was to find docked molecules that ranked highly for both paired targets, something that seemed challenging but plausible. While two of the pairs, α_{2A} and SERT and SERT and MOR, involve targets from different fold families, and the third pair, MOR and α_{2A}, differed in the size of their orthosteric sites, all three shared ligand recognition properties, including a key aspartic acid with which a cationic ligand group interacted, and patches of aromatic residues that recognized ligand aryl groups (Figure 2).

The same docking parameters were used as in previous single-target studies,[36,37,48] with make-on-demand molecules docked from the ZINC22 database. Maintaining the sampling and scoring from the previous studies had the dual advantage of exploiting what had been successful docking campaigns, most of which had featured relatively high hit-rates and relatively potent docking hits, and it allowed us to compare single-target results to those with dual-target docking used here.

Briefly, against the SERT/MOR pair, about 900 million cationic molecules were docked in over 3 trillion configurations, while against the α_{2A}/SERT and α2/MOR we were restricted to fragment-like molecules by the size of the α_{2A} pocket, limiting us to 33 million cations fit in about 50 billion configurations, all using DOCK 3.8 and scored using its physics-based scoring function. The top million compounds were collected from each campaign and 110,000, 117,000 and 500,000 shared compounds were identified for the pairs α_{2A} and SERT, MOR and α_{2A}, and SERT and MOR respectively. After eliminating molecules adopting strained conformations, those that left hydrogen-bond donors unsatisfied in the docked complex, or that missed one of a few of key interactions (e.g., an ion pair within 3.2 Å of the conserved Aspartate), 908, 819, and 280 potential polypharmacological compounds remained for each of the three pairs, respectively. These were visually inspected for a final selection of compounds to synthesize and test (Figure 3).

Ultimately, 104, 55, and 82 compounds that were jointly high ranking among the 900 million docked compounds were de novo synthesized and tested for the α_{2A} and SERT, SERT and MOR, and MOR and α_{2A}, respectively (Table 1). The selected compounds were always ranked among the top 0.1% for their particular docking campaign. Inevitably, with so many compounds docked, there was a spread of compounds between the ranks for the two targets. For α_{2A} /SERT, ranks for α_{2A} varied from 16 to 996,834 while those for SERT they varied from 2632 to 995,729. For MOR/α_{2A}, α_{2A} ranks varied from 2,912 to 113,673 while those for MOR they varied from 2,569 to 994,834. For SERT/MOR, SERT ranks varied from 2 to 997,841 while those for MOR they varied from 392 to 998,570. With the constraint of finding dual-targeting ligands, we accepted ligands with lower percentile ranks than would be typically considered in a single-target campaigns.[36,37,48]

Table 1. Polypharmacology and Single-Target Hit Rates

	α_{2A}/SERT	SERT/MOR	MOR/α_{2A}
Synthesized	104	55	82
Binders	41[a]/21[b]	26[b]/16[c]	3[c]/13[a]
Hit Rate	39%[a]/20%[b]	47%[b]/29%[c]	4%[c]/16%[a]
Dual binders	16	6	0
Agonist activity	5	1	0
K_i of best compound (nM)	180[a]/198[b]	830[b]/1,418[c]	
Previous hit rate	35% (α_{2A})	36% (SERT)	30% (MOR)

[a]The experimental hit-rate for α_{2A}. [b]The experimental hit-rate for SERT. [c]The experimental hit-rate for MOR.

Compounds were first tested in radioligand displacement assays at 10 μM for α_{2A}, 30 μM for SERT, and at 100 μM for MOR. For those compounds with greater than 50% displacement at these concentrations, full concentration−response curves were measured (SI Figure 5). Those that had apparent K_i values <5 μM were progressed to functional studies for the α_{2A} and MOR (SI Figures 6 and 7). α_{2A} agonism was assessed in full concentration−response using a BRET G_i activation assay,[48] while for the MOR agonists a GloSensor cAMP accumulation assay was used, again in concentration response (Methods).

We had previously docked to all three of α_{2A}, SERT, and MOR as individual targets[36,37,48] and it seemed interesting to compare the experimentally confirmed hit rates (number active/number experimentally tested) from the original single target docking to the new joint-target docking conducted here. By adding a second constraint—the need to rank well at both targets—one might expect hit rates to decline. While this was sometimes true, it was not always the case. In the screen against SERT and α_{2A}, the SERT hit rate dropped to 20% from the 36% in docking to SERT alone,[36] but in the polypharmacological screen with MOR the hit rate against SERT rose to 49%. In the MOR and α_{2A} campaign, hit rates dropped versus targeting each receptor alone, but were about the same when each was jointly targeted with SERT (Table 1). While some caution is warranted when comparing hit rates, as in our workflow there is a human component at the final stage of compound selection, still, it may be that the higher than expected joint hit rates may reflect the larger library used here than in the original studies, as hit-rate

https://doi.org/10.1021/acs.jmedchem.5c03810
J. Med. Chem. 2026, 69, 6210−6229

Table 2. Potent Prospective Docking Hits for α_{2A}/SERT and SERT/MOR[a]

ID (Short Code)	Structure	SERT K_i (nM)	α_{2A} or MOR[b] K_i /EC_{50} (nM)
ZINCfn000001cc10 ('cc1O)	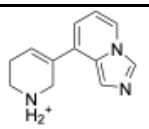	1,300 ± 350	2,100 ± 360 / 2,200 ± 960
ZINCfn0000010wdh ('0wdh)	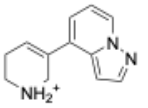	12,400 ± 500	1,500 ± 350 / 1000[a]
ZINCgv000000zHhp ('zHhp)	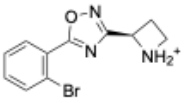	10,200 ± 5,300	2,500 ± 100 / 960[a]
ZINCgw000000A08w ('A08w)	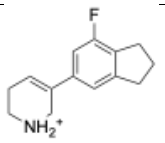	2,200 ± 800	310 ± 40 / 490 ± 225
Z8779877149 ('Z7149)	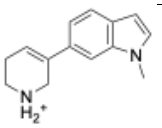	198 ± 100	180 ± 43 / 440 ± 170
ZIN00000dBlqj ('BIqj)	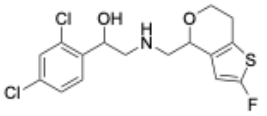	830 ± 145	1,418 ± 700[b]
ZINn|000005H8Oo ('H8Oo)	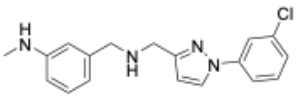	551 ± 110	1,393 ± 157[b]
ZINCil000002o16P ('o16P)	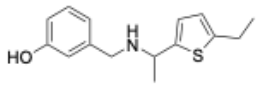	2,590 ± 650	1,228 ± 150[b]
ZINCmK000003XTlt ('XTlt)	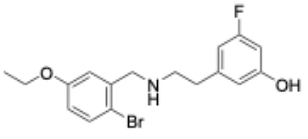	3,595 ± 750	1,120 ± 147[b]
ZINCnR000004amQ1 ('amQ1)	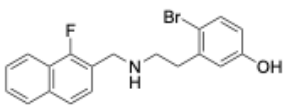	258 ± 50	4,082 ± 385[b]
ZINCnK000005PogF ('PogF)	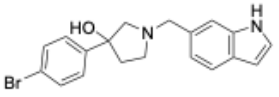	193 ± 33	32 ± 13 μM[b]

[a]K_i was measured by radioligand displacement in full concentration−response. α_{2A} agonism was assessed in full concentration−response using a BRET G_i activation assay while for the MOR agonists a GloSensor cAMP accumulation assay was used, again in concentration response (Methods). Data are mean ± s.e.m. [a]The E_{max} is below 20%, and the corresponding EC_{50} exhibits a large standard deviation. [b]K_i for MOR; all ligands above '**BIqj** are α_{2A} ligands.

https://doi.org/10.1021/acs.jmedchem.5c03810
J. Med. Chem. 2026, 69, 6210−6229

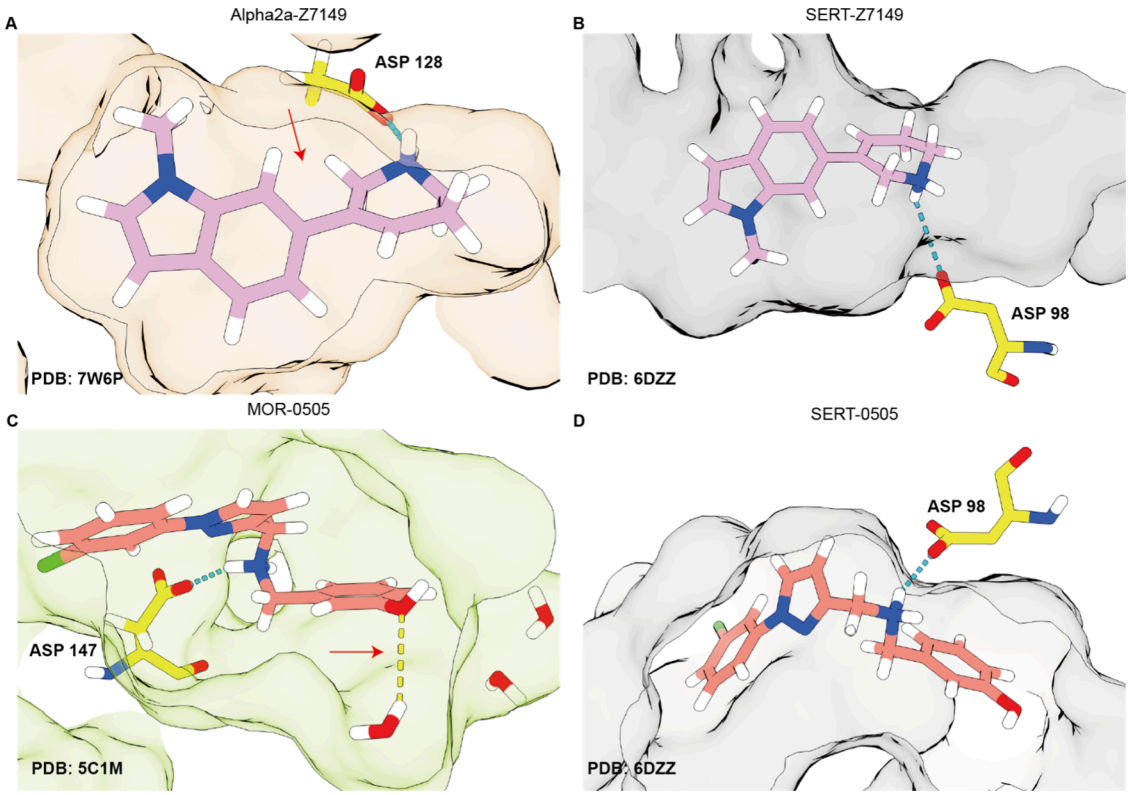

Figure 4. The docking-predicted poses of z7149 and 0505. (A) **z7149** in the α_{2A} orthosteric binding pocket. The red arrow points to the only position where compound elaboration is sterically permitted. (B) **z7149** in the SERT pocket. (C) **0505** in the MOR pocket. The red arrow points at a putative hydrogen-bond between the ligand and an ordered water in MOR. (D) **0505** docked in the SERT pocket. The key hydrogen bond with the aspartate is shown in blue. Docking to the same PDB structures as in Figure 2.

often improve with library size.[59,60] Indeed, such behavior with library size was a motivation for this study.

If hit rates were often maintained on a target-by-target basis, the potency for the docking hits was typically worse for the dual activity ligands than for those from the single target docking studies.[36,37,48] For instance, when targeting the α_{2A} receptor alone, the most potent ligand was a 10 nM agonist[48] while the most potent α_{2A} agonist here was 390 nM. Similarly, the most potent SERT inhibitor found from single target docking had a K_i of 29 nM while the most potent here had K_i values in the 200 nM in range. For MOR, the ligand with the highest K_i was of 2.3 μM when targeted alone,[37] while the highest here was 725 nM. However, the former screen only involved 3 million molecules, several orders-of-magnitude smaller than the current study. Only one docking hit from the dual MOR/SERT campaign had weak agonism.

Naturally we were ultimately seeking ligands with *joint* activity, and here hit rates did decline versus the individual target docking campaigns. Whereas 41 docking-prioritized molecules bound to α_{2A} (39% hit rate), and 21 bound to SERT (20% hit rate), only 16 bound to both (15% joint hit rate). For SERT and MOR polypharmacology, the respective numbers were 26 for SERT (47%), 16 for MOR (29%), but only 6 for both (12% joint hit rate). For MOR and α_{2A}, no joint acting ligands were found at all, likely reflecting the low hit rates for both (accordingly, we did not further advance molecules from this pair). The rate of dual binding was 2-fold better for α_{2A}/SERT than might be predicted from simple multiplication of the individual hit rates, though whether this was statistically significant is uncertain. More confidently, the rate of dual binding seems far better than simply taking hits from the SERT alone docking campaign and testing them for α_{2A} activity,[36] or by taking the actives from the campaign against α_{2A} alone and testing them against SERT;[48] in both cases, none were active up to 10 μM.

A final criterion of polypharmacology is function, and here we sought α_{2A} and MOR receptor agonists. Of the 16 ligands with joint activity against α_{2A} and SERT, five were α_{2A} agonists (Table 2), while of the six ligands that bound to MOR and SERT, only one was a MOR agonist (Table 2).[35,48] Agonist EC_{50} values ranged from 390 nM to 2.2 μM for α_{2A}, and was weak for the MOR. Since we only found one MOR agonist, and because we had previously found that nonagonists can reveal agonism on optimization and stereochemical purification,[38] we advanced all six joint activity ligands for MOR. In summary, the successive constraints of seeking: (**1**) < 10 μM ligands on the single targets to (**2**) joint target binding, to (**3**) agonist activity against the receptors, despite often favorable success rates at each step, left us in the end with five polypharmacology ligands for α_{2A}/SERT and one for MOR/SERT out of 241 tested. Adding another five nonagonists from the MOR/SERT screen brought us to 11 polypharmacology ligands to progress.

Optimization of Docking Hits

To optimize our initial hits, we first sought positions where modifications did not appear clash with either target (Figure 4A–D) and modeled ligand. With the different topologies between the transporter SERT and the GPCRs α_{2A} and MOR, there were only a few such positions on the docked ligands. For instance, the compound **Z8779877149** ('**z7149**) was deeply buried in the α_{2A} pocket (Figure 4A) limiting molecule growth, whereas the much larger binding cavity of SERT allowed for modifications at more positions (Figure 4B), and the union of

https://doi.org/10.1021/acs.jmedchem.5c03810
J. Med. Chem. 2026, 69, 6210−6229

Table 3. Characteristic Analogs for α_{2A}/SERT from Five Initial Hits[a]

ID (Short Code)	Structure	SERT K_i (nM)	α_{2A} EC_{50} (nM)
Z4387158014 ('8014)	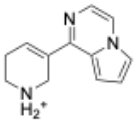	Don't bind	170 ± 12
Z8727393901 ('3901)	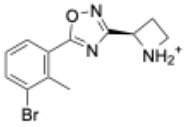	65 ± 10	Not agonist
Z8763389252 ('9252)	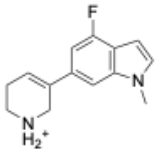	1600 ± 700	9% @ 30μM[a]
Z8763389236 ('9236)	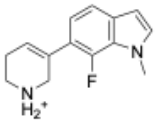	440 ± 60	21% @ 30μM[a]
Z1262606886 ('6886)	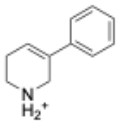	5,100 ± 1,700	61 ± 7

[a]K_i was measured with radioligand displacement assays and full concentration−response curves were collected. α_{2A} agonism was assessed in full concentration−response using a BRET G_i activation assay (Materials and Methods). Data are mean ± s.e.m. [a] Compound exhibits very weak α_{2A} agonism.

the two constraints naturally left only one position that could accommodate modifications (Figure 4A,B). In a second approach, we first made small, systematic changes to the ligands irrespective of the receptor structures. We then searched a 20 billion make-on-demand library with the Arthor and Small-World programs (https://sw.docking.org/, NextMove Software, Cambridge UK), finding 11,018 synthesizable analogs for the 11 parents. These were prioritized by docking them into the paired receptors, seeking those with favorable fits. From the two approaches, 171 analogs were synthesized for the 11 parents in a first optimization round (SI file *verified-compounds.xlsx*).

For the α_{2A}-SERT pair, we focused on the five most potent ligands in two different chemotypes (Table 3). For the first chemotype, we found analogs with 6-fold improvement on α_{2A} (compound **Z4387158014**), while for the second we found molecules with up to 150-fold improved SERT inhibition (compound **Z8727393901**), but in both cases at the cost of losing activity on the other target (Table 3). For the third chemotype, represented by parents '**z7149** and **ZINCg-w000000A08w** ('**A08w**), we only found analogs that maintained joint target activity, but did not improve it. Eventually, six compounds, two parents from docking and four analogs, were progressed into pharmacokinetic studies (SI Table 1). The initial docking hit '**z7149** emerged with the best on-target activity and CNS exposure.

'**z7149** is a tetrahydropyridine, a class which we had discovered as active against 5-HT_{2A} with antidepression-like activity.[38] Because 5-HT_{2A} has been implicated in analgesia[61,62] and because SERT inhibitors are well-known as antidepressants, we thought it interesting to test for '**z7149**'s activity against 5-HT_{2A}. Encouragingly, '**z7149** was active at 5-HT_{2A} in the same concentration range as for α_{2A} and SERT, with an agonist EC_{50} of 172 nM and an E_{max} of 76% based on G_q calcium assay. These characteristics was not far from what we had seen in the tetrahydropyridine-5-HT_{2A} project, from which efficacious and long lasting antidepressant-like compounds had emerged.[38] Both the on-target potency of '**z7149** against α_{2A}, SERT, and 5-HT_{2A}, and its relatively favorable CNS exposure motivated us to test '**z7149** in both analgesia, antidepressive, and anxiolytic drug-like assays, to which we will return.

For the SERT-MOR pair, we focused on the six most potent hits, representing five different chemotypes (Table 2). The larger MOR binding cavities (Figure 4C,D) allowed more freedom to derivatize. Among the modifications, we changed the *N*-methylaniline to a phenol to improve hydrogen bonding with the ordered waters in the MOR orthosteric site (Figures 4C and Table 4), i.e., compound **Z8962410505** ('**0505**). Encouragingly, this converted an antagonist into an agonist while also improving its SERT activity by 6-fold. Subsequent changes did not improve activity further and this compound, '**0505,** was progressed into pharmacokinetic studies (Table 4).

Taking the α_{2A}/SERT and SERT/MOR target pairs together, 254 analogs were synthesized for 11 docking hits. While for individual targets within the pairs ligand affinities improved by between by 4- to 150-fold over parent compounds, improvement against one target often came at the cost to activity on the second (Table 3). The best case was for SERT/MOR, where replacing a methyl aniline with a hydroxyl improved affinity about 6-fold for both targets (compound '**0505**), reaching a K_i of 250 nM for SERT and an agonist EC_{50} of 140 nM for MOR.

https://doi.org/10.1021/acs.jmedchem.5c03810
J. Med. Chem. 2026, 69, 6210−6229

Table 4. Optimization of the SERT/MOR Docking Hit H8Oo[a]

ID (Short Code)	Structure	SERT K_i (nM)	MOR EC_{50}
Z8962410505 ('0505)	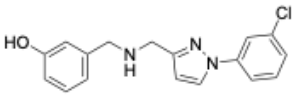	252 ± 45	140 ± 50
Z733945210 ('5210)	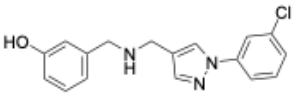	915 ± 40	330 ± 100
Z9118220851 ('0851)	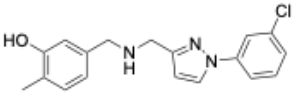	330 ± 20	33 μM[a]
Z9118220854 ('0854)	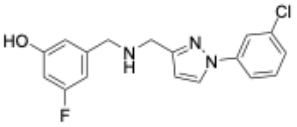	530 ± 50	12 μM[a]
Z9118220870 ('0870)	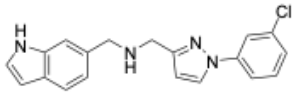	200 ± 30	35 μM[a]
Z973094722 ('4722)	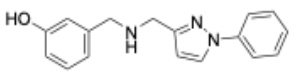	1,430 ± 140	Not agonist
Z9118220860 ('0860)	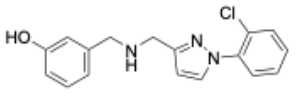	1,100 ± 50	Not agonist
Z9118220862 ('0862)	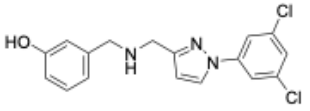	75 ± 4	Not agonist
Z9118220861 ('0861)	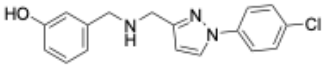	240 ± 60	Not agonist

[a]K_i was measured with radioligand displacement assays and full concentration−response curves were collected. MOR agonism was assessed in full concentration−response using GloSensor cAMP accumulation assay (Materials and Methods). Data are mean ± s.e.m. [a] The compound exhibits a large standard deviation and weak MOR agonism.

Even here, subsequent analoging failed to further improve joint (Table 4), and for both pairs of targets, ligand activities plateaued in the 100 nM range.

Off-Target Effects

Ideally, polypharmacology compounds will be selective against off-targets and not simply gain their polypharmacology from promiscuity. We thus evaluated inhibition at the transporters DAT and NET, which are closely related to SERT. '**z7149** had K_i values of 6.3 μM and 881 nM on DAT and NET, respectively, while '**0505** had K_i values of 922 nM and 3.2 μM, respectively (SI Figure 8). Both compounds were also tested for agonism at 320 human GPCRs in the Tango assay at 10 μM. Little activity was detected against any target for '**0505**, while '**z7149** only showed substantial activity versus the 5-HT_{2B} (EC_{50} = 15 nM, E_{max} = 34%) and 5-HT_{2C} receptors (EC_{50} = 26 nM, E_{max} = 19%). From a therapeutic perspective, the potency on 5-HT_{2B} is concerning, owing to its role in valvular pathologies,[63,64] something that partly ameliorated by low efficacy. Overall, the molecules were not broadly promiscuous in these assays.

Structure Determination by cryo-EM

To template future compound optimization, understand activity at atomic resolution, and to test the docking predictions, we determined the structures of α_{2A} and SERT bound to '**z7149**, and of MOR bound to '**0505**, using single-particle cryo-EM (Methods). Structures were determined to between 3.29 Å and 3.40 Å global nominal resolutions, and to resolution ranging from 3.3 Å to 3.6 Å in the orthosteric sites of the receptors and transporter. The cryo-EM maps yielded well-defined and contiguous TM densities that allowed for unambiguous modeling of the orthosteric regions and of the bound ligands.

The cryo-EM model for '**z7149** bound to α_{2A} superposed with the docking pose with a ligand heavy atom root-mean-square deviation (RMSD) of 1.22 Å (Figure 4A), ion-pairing with Asp128 as predicted. In the SERT cryo-EM structure with

https://doi.org/10.1021/acs.jmedchem.5c03810
J. Med. Chem. 2026, 69, 6210−6229

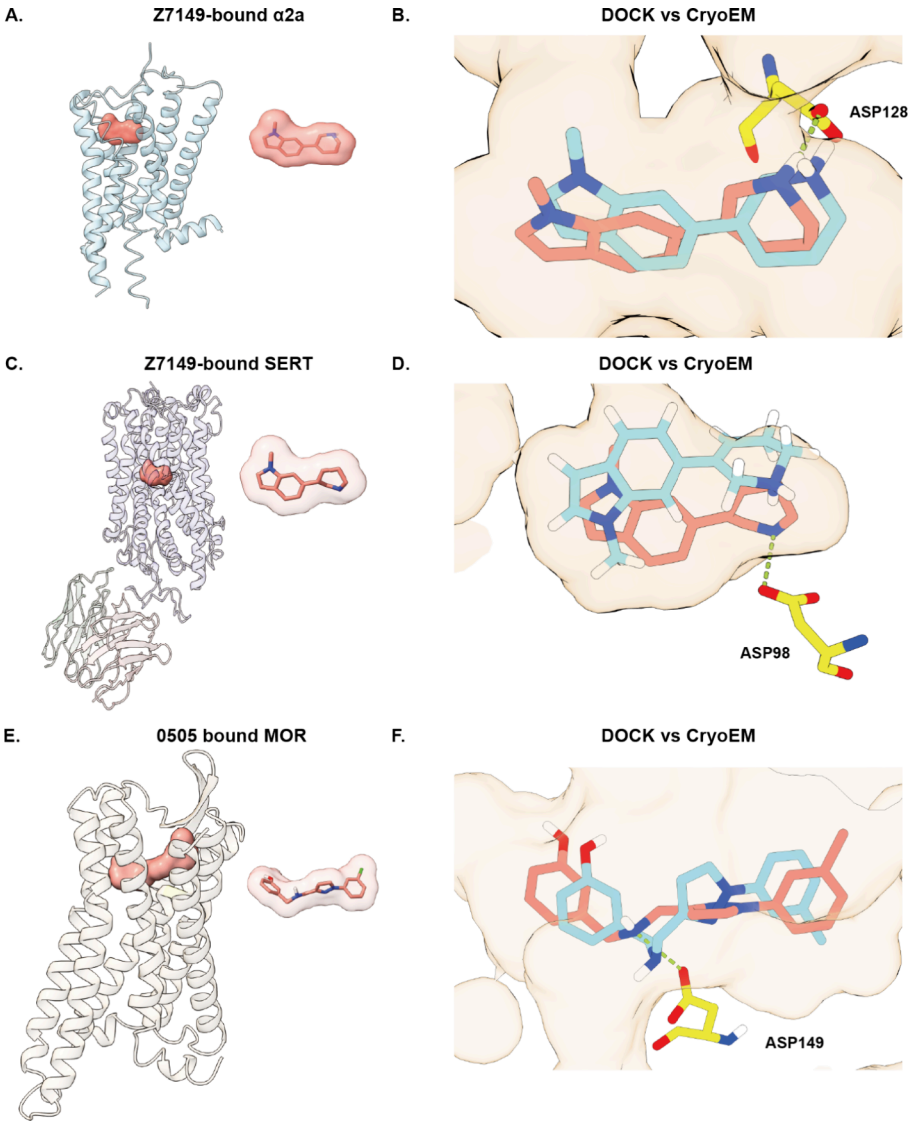

Figure 5. Cryo-EM structures and comparison to the docking predictions. (A) The cryoEM of **z7149**-bound α_{2A} structure (PDB ID: 9PQD) and the corresponding density for **z7149**. (B) The **z7149** cryoEM (carbons in pink) suprerposed on that predicted by docking (carbons in cyan) in the binding pocket. (C) The cryoEM of **z7149**-bound SERT structure (PDB ID: 9PNS) and the corresponding density for **z7149**. (D) The **z7149** cryoEM (carbons in pink) suprerposed on that predicted by docking (carbons in cyan) in the binding pocket. (E) The cryoEM of '**0505**-bound MOR structure (PDB ID: 9PPQ) and the corresponding density for '**0505**. (F) The '**0505** cryoEM (carbons in pink) suprerposed on that predicted by docking (carbons in cyan) in the binding pocket. The key aspartic acid is shown in yellow. And the corresponding key interaction is shown in green. The receptor amino acid is shown in wires.

'**z7149**, the receptor adopts a closed-occluded conformation, where transmembrane helix 1 (residues 85−95) swings into the orthosteric site. As previously,[36] the docking campaign was launched against the inward-open state conformation of SERT. Despite the receptor conformational change, the docking-predicted pose interacts with the same residues and the same site as observed in experimental model (Figure 5C); partly because of the conformational change, the ligand RMSD of the docked to the experimental pose rose to 2.97 Å. However, if we selected the higher docking conformation pose of '**z7149**, we could have the ligand RMSD to 1.91 Å. Compared with the docked model (Figure 4B), the occluded conformation has a smaller cavity (Figure 5D) consistent with reduced potency of larger analogs like **Z8763389252** (Table 2). Comparing the α_{2A} and SERT complexes of '**z7149**, the tetrahydropyridine rotates to orient its cationic nitrogen atom into different relative positions to hydrogen bond with Asp128 (in α_{2A}) or with Asp98 (in SERT), an ability that may be beneficial for polypharmacology between targets unrelated by sequence.

Turning to the MOR/'**0505** complex, the ligand cryo-EM map also broadly supports the docking pose. In the experimental complex, '**0505** hydrogen-bonds with Asp149 and the ordered waters, as predicted, in what is normally the phenol recognition site of the receptor. The experimental geometry superposes with the docked with a root-mean-square deviation (RMSD) of 2.1 Å (Figure 5E).

In Vivo Activity of the Polypharmacology Compounds

Whereas the potency of '**z7149** and '**0505** was 10- to 30-fold weaker than we might typically use for *in vivo* active probes, their polypharmacology could lead to new or enhanced activity versus single-target drugs. Accordingly, we first investigated their pharmacokinetics, asking if the compounds were well-exposed in the brain. Both had substantial CNS exposure following a 10

https://doi.org/10.1021/acs.jmedchem.5c03810
J. Med. Chem. 2026, 69, 6210−6229

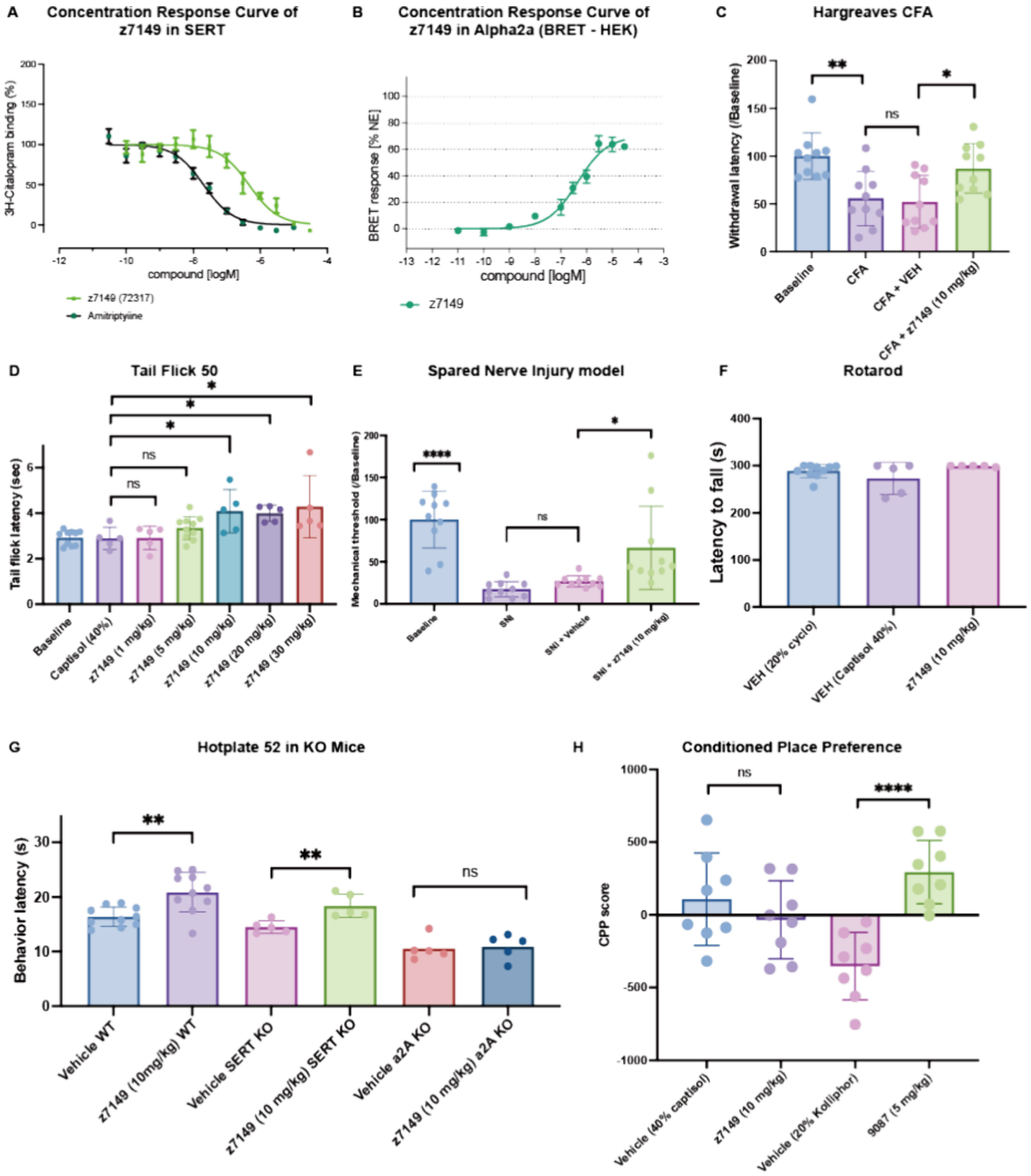

Figure 6. '**z7149** is antinociceptive and antiallodynic and does not induce sedation or conditioned place preference (CPP) in mice. (A) '**z7149** is a 440 nM α_{2A} agonist and (B) a 180 nM SERT inhibitor. The compound reduces CFA-induced thermal hypersensitivity (C) in the Hargreaves test at 10 mg/kg. (D) '**z7149** dose-dependently produced analgesia in the tail flick assay. (E) '**z7149** also reduces spared nerve injury (SNI)-induced mechanical allodynia. (G) The antinociceptive effect of z7149 in the hot plate test is α_{2A} but not SERT-dependent. '**z7149** did not produce sedation (motor impairment) in the rotarod test (F) and did not induce CPP (H).

mg/kg dose (i.p.), reaching C_{max} values of 79.7 μMol (z7149) and 14.8 μMol ('**0505**), with half-lives of 56 and 117 min, respectively (SI Figures 9−21 and Table 1). However, their cerebrospinal fluid (CSF) exposures, which are a proxy for free fraction in the brain[65,66] were lower, reaching 830 nM for '**z7149** and only 27 nM for '**0505**. This result corresponds to a 2- to 4-fold coverage over '**z7149's** EC_{50} against α_{2A}, SERT, and 5-HT_{2A} at C_{max}, but less than 0.3-fold for '**0505** relative to its MOR and

https://doi.org/10.1021/acs.jmedchem.5c03810
J. Med. Chem. 2026, 69, 6210−6229

SERT activities. This level of coverage is too low to make in vivo activity likely for '**0505**, and indeed in preliminary antinociception assays we found little activity for this compound (SI Figure 9). Accordingly, '**0505** was not further pursued.

The PK properties of '**z7149** were more encouraging, and we observed antinociceptive and antiallodynic activity in behavioral assays after IP dosing at 10 mg/kg. The tests include the tail flick (50 °C) and Hargreaves test, which measure reflex response to a noxious stimulus, the hot-plate, which measures both reflex and affective responses (e.g., licking) to noxious heat applied to all four paws, the spared nerve injury model of neuropathic pain and the Complete Freund's Aduvant (CFA) model of inflammatory pain (Figure 6). Encouragingly, and akin to other docking-derived α_{2A} agonists like '**9087**,[48] '**z7149** was not sedating as measured in the rotarod assay, suggesting that its antinociceptive action was not due to motor impairment or sedation. In contrast to '**9087**, '**z7149** did not induce conditioned place preference. This difference may reflect the polypharmacology of '**z7149** on SERT, the inhibition of which can suppress CPP,[67,68] an activity that '**9087** lacks.[48] We note that we have not demonstrated cause and effect here, and the role of SERT in the lack of CPP for '**z7149** must be for now considered speculative (Figure 6).

Owing to its joint 5-HT_{2A} and SERT activity, we also tested '**z7149** for anxiolytic- and antidepressant drug-like activities in mice (Figure 7A–C). In a four-plate assay that assesses punished crossings by foot-shock, mice receiving (i.p.) 0.25 mg/kg '**z7149** crossed almost twice as often as did those treated with vehicle, achieving almost the same anxiolytic drug-like effect as with the positive control diazepam dosed at 0.5 mg/kg (i.p.). Meanwhile, in the tail suspension assay, mice heterozygous for the VMAT2 deletion, which are prone to a depressive-like phenotype,[69] 0.2 and 0.5 mg/kg doses of '**z7149** had antidepressant drug-like effects for up to 5 days. Both the strength and the longevity of the effect may be compared favorably relative to fluoxetine, which at 100-fold the dose of '**z7149** was at best as acutely efficacious as the new polypharmacology ligand (Figure 7C, 30 min timepoint), while fluoxetine's efficacy declined over time and was lost by day 3. If the long-lasting effect of 5-HT_{2A} tetrahydropyridine agonists is precedented,[38] the potency of the effect, given the low pharmacokinetic coverage of '**z7149** (EC_{50}/C_{max}) versus the earlier series, may reflect the dual engagement of both 5-HT_{2A} and SERT, the latter of which was not meaningfully inhibited by the earlier series. Similarly, the apparent anxiolytic drug-like effect of the molecule may also reflect its polypharmacology. We note that while efficacy improved in dose response up to 0.5 mg/kg, it declined at 1 mg/kg, which might reflect a negative aspect of the polypharmacology of '**z7149** via its α_{2A} agonism, as α_{2A} *antagonism* is thought to have antidepressant effects.[70] Here again, the role of joint 5-HT_{2A} agonism/SERT inhibition in the in vivo efficacy has not been mechanistically shown.

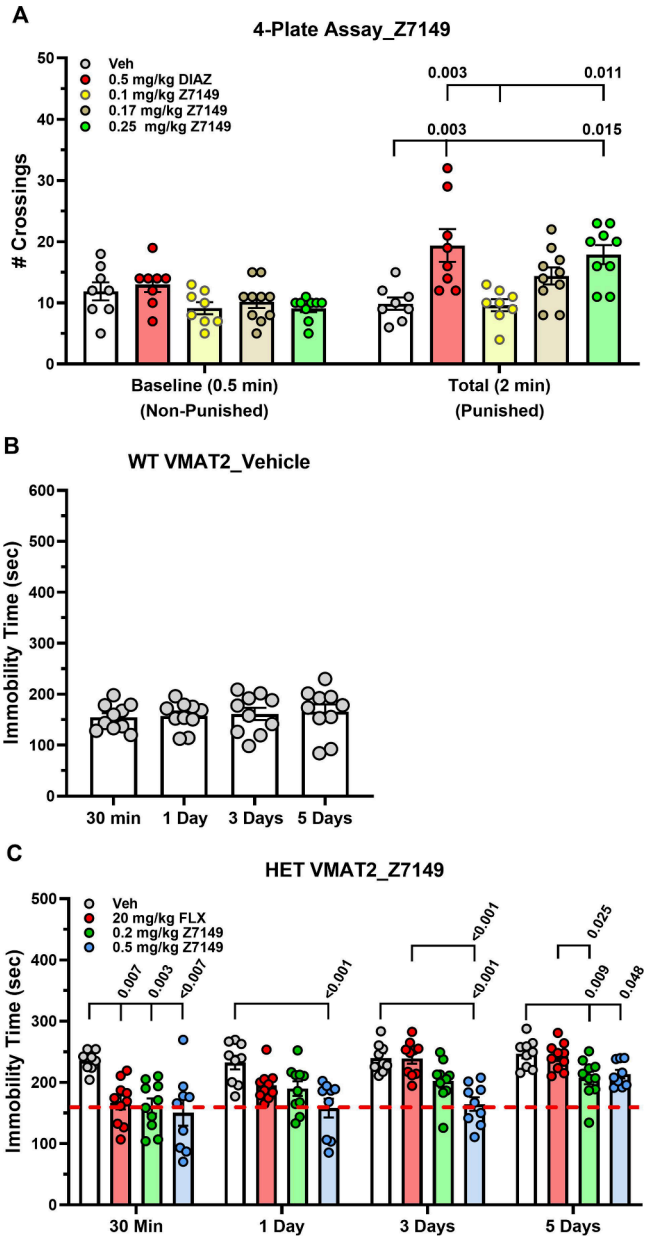

Figure 7. Anxiolytic-like and antidepressant drug-like effects of 'z7149 in mouse behavioral assays. (A). '**z7149** and the positive control anxiolytic, diazepam, increase punished crossings in the four-plate assay, producing an anxiolytic-like effect. (B). Immobility in the tail suspension assay is low in WT VMAT2 mice treated with vehicle. This represents the maximum immobility control effect in the HET VMAT2 HET model (dotted red line). (C). Reduction of immobility in tail suspension over several days in HET VMAT2 mice by '**z7149** compared to the positive control drug fluoxetine (20 mg/kg i.p.). Fluoxetine and both doses of '**z7149** are active acutely. Like other molecules with 5-HT_{2A} agonist activity, the antidepressant drug-like activity of 0.5 mg/kg '**z7149** lasts for several days. The data are presented as means and standard errors of the mean. In each panel statistical comparisons are made between or among groups denoted by *posthoc p*-value above a bar as compared to the bar without a statistical value. All statistics and the numbers of mice in studies can be found in SI Table 2.

DISCUSSION

Large library, multitarget docking yielded molecules with joint activity against double and triple target combinations. Four observations deserve emphasis. First, as docking libraries expand, more likely poly pharmacological compounds fortuitously appear (Figure 1 and SI Figure 1), and in retrospective dual target docking these are highly ranked in both targets (SI Figures 2~4). Second, in prospective dual target docking against biologically relevant but structurally different targets, multiple ligands that bind to both targets were found. While the tertiary structures of these molecular target pairs differ, their binding sites retain similarities and are similar in size. Conversely, for MOR/α_{2A} the size of the orthosteric sites differed, and few joint-binding ligands were found; here, docking could not overcome inherent physicochemical property mismatches between the

https://doi.org/10.1021/acs.jmedchem.5c03810
J. Med. Chem. 2026, 69, 6210−6229

sites. Third, even for pairs where multiple hits were found, structure-based optimization was more challenging than we had experienced in single target campaigns against each target individually.[36,37,48] While analoging led to up to 150-fold improvement for an individual target, it was rare for a molecule to improve against both targets; more typically, improvement against one target was accompanied by loss of activity against the other. Fourth, despite relatively modest joint activity, at least one molecule, '**z7149**, was active in antiallodynia and possessed anxiolytic and antidepressive drug-like actions in mouse assays. Its lack of conditioned place preference separates '**z7149** from compounds like '**9087**, which came from earlier, single target campaigns, and may reflect the new engagement of SERT. Similarly, '**z7149's** potent antidepressant and anxiolytic drug-like activities may reflect the engagement of SERT in addition to 5-HT_{2A} activity.

Certain caveats should be mentioned. Neither '**z7149** nor '**0505** are as potent as single target agonists from earlier studies.[37,48] This partly reflects beginning with less potent docking hits and even more the challenges of multiparameter optimization (here, optimizing against two targets simultaneously). Similarly, compound pharmacokinetics was worse than for the earlier, single-target molecules, likely also reflecting the constraints of multitarget optimization and the lack PK property calculation early of our ligand prioritization pipeline—an active area of research. Methods like generative AI[71,72] or machine learning[73−75] with their ability to take guided searches through very large spaces, hold promise here but remain lightly tested prospectively. As in the single-target campaign against SERT, whereas the docked ligand occupied the correct site and made most of the interactions observed in the experimental structure we subsequently determined, the global conformation of the transporter changed from the inward-open structure that we had docked against. Here again, more advanced treatments, including flexible receptor docking, hold promise, though the challenge remains the introduction of decoy structures in the context of a large library campaign.[76−78] Finally, as many of our more potent molecules remain relatively small, we cannot rule out multiple binding modes, though the ionic interaction common to these targets might tilt against this.

Overall, a mixed picture emerges. Against pairs of targets related by grossly similar binding sites, but adopting different folds, large library docking found molecules that ranked highly against both with relatively high hit rates against each individual target. Hit rates fell when we insisted that a ligand be active on both targets, and the jointly active ligands were only active in 100 nM to low μM range, weaker than the most potent molecules from single-protein campaigns against the same targets.[36,37,48] Also, we achieved only modest success in jointly optimizing these actives, and only one molecule emerged with *in vivo* efficacy, '**z7149.** This compound did show new therapeutic activities that may arise from its polypharmacology: '**z7149** was effective in acute and chronic pain models without inducing the conditioned place preference that was characteristic of earlier agonists that lacked the SERT activity of the new molecule. '**z7149** also had potent antidepressant and anxiolytic drug-like activity, despite its relatively low potency to exposure ratio in the CNS, which may reflect its joint activity on SERT and 5-HT_{2A}. Thus, while this work teaches that library docking can address diseases where polypharmacology is advantageous, even when the targets are not in the same family, the constraint of dual receptor targeting worsens outcomes at every stage of ligand discovery and optimization. It may be that these deficits will be overcome by further growth of docking accessible libraries, which now stretch into the trillions. Conversely, for proteins whose dual engagement is advantageous, but different by fold, a polypharmacy approach may also warrant investigation.

MATERIALS AND METHODS

Molecular Docking

The docking parameters were maintained in previous single-target studies, with make-on-demand molecules docked from the ZINC22 database: 33 million compounds were docked against α_{2A}/SERT and α_{2A}/MOR, and 900 million compounds were docked against SERT/MOR. The shared 300,000 top-ranking molecules were filtered for novelty using the ECFP4-based Tanimoto coefficient (Tc < 0.35) against known ligands for each target. We used interaction fingerprint filtering to remove compounds that geometrically missed key interactions, or that exposed uncompensated hydrogen bond donors, focusing on the hydrogen bond between Asp98 (SERT), Asp128 (α_{2A}) and Asp149 (MOR). A strain filter was set to >2 kcal/mol to remove conformations with high internal energies. The remaining molecules were further clustered topologically using an ECFP4-based Tanimoto coefficient (Tc) of 0.5, resulting in ∼ 1000 high-ranking cluster representatives for visual inspection in both binding pockets. Compounds with favorable interactions with both targets were prioritized for *de novo* synthesis and testing.

Compound Synthesis and Purity

All compounds tested were synthesized and purified by Enamine (see synthesis and purification section in the SI). All compounds were at least 90% pure by LC/MS, and active compounds were confirmed by subsequent ^{1}H NMR. The purity of active compounds ranged from 90 to more than 95% by LC/MS and ^{1}H NMR, with 196 of the 248 molecules active on any target, 95% pure or better, while of the 71 molecules jointly active on two or more targets (≤10 μM on each), 59 were 95% pure or better. All compounds that progressed into pharmacokinetic and *in vivo* behavioral studies were at least 98% pure.

Ligand Optimization

In a first-round analoging, primary docking hits (Figure 3) were used as queries in the SmallWorld (https://sw.docking.org/) and Arthor (http://arthor.docking.org) programs (NextMove Software, Cambridge UK) of a 20 billion molecule Enamine REAL set, and molecules with up to three heavy atom changes from the parents were collected. These were docked for complementarity, as above, and well-fit analogs were prioritized and tested. For all three targets, two further rounds of analogs were selected, guided by the affinity changes observed in the first round and occasionally to test specific interaction hypotheses.

α_{2A} Radioligand Binding

Binding affinities for the α_{2A} receptor were determined as described.[48] In brief, membranes were prepared from HEK293T cells transiently transfected with the cDNA for the human α_{2A}, murine α_{2A} (provided by Yang Du, ShenZhen, China). The receptor density (B_{max} value) and the specific binding affinity (K_d value) for the radioligand [^{3}H]RX82,1002 (specific activity 51 Ci/mmol, Novandi, Södertälje, Sweden) were determined as 1600 ± 340 fmol/mg protein and 0.56 ± 0.03 nM, respectively.

Competition binding with α_{2A} was performed by incubating membranes in buffer A (50 mM Tris at pH 7.4) at final protein concentrations of 3 to 10 μg per well with the radioligand (final concentration 0.5 nM) and varying concentrations of the competing ligands for 60 min at 37 °C. Protein concentration was measured using the method of Lowry.[79,80]

The resulting competition curves were analyzed by nonlinear regression with Prism10 (GraphPad Software, San Diego, CA) to provide mean inhibitory concentration (IC_{50}) values, which were subsequently transformed into a K_i values using the Cheng and Prusoff eq (72). Mean K_i values (±SEM for $n \geq 3$ or ± SD for n = 2) were derived from 2 to 7 independent experiments, each performed in triplicate.

https://doi.org/10.1021/acs.jmedchem.5c03810
J. Med. Chem. 2026, 69, 6210−6229

MOR Radioligand Binding

Radioligand competition assays were performed as previously[58] derived from earlier protocols.[37,38,81] Membrane preparations were harvested from HEK293T cells transiently expressing full length human MOR (pCDNA3.1 vector plasmid) following the Lipofectamine 3000 Reagent transfection system (Thermo Fischer). A binding affinity for the membrane preparation of 2.0 nM was measured for a ^{3}H-naltrexone radioligand (PerkinElmer) in a saturation experiment adjusted for nonspecific binding as measured in the presence of a saturating concentration of 33 μM unlabeled naloxone. Radioligand competition was performed in 96 well V-PP coated plates. Each well contained 200 μL of homogeneous membrane solution in binding buffer (50 mM HEPES, 0.1 mM EDTA, 10 mM MgCl2, 0.1% BSA, pH 7.4), 25 μL of a 10x ^{3}H-naltrexone dilution, and 25 μL of a 10x dilution of the ligand being tested. For the ^{3}H-naltrexone dilution, a small volume of the stock solution (1 mCi/mL in ethanol) was diluted with room temperature binding buffer to achieve a final radioligand concentration of 2.3 nM in each well. For test ligands, dry powders were dissolved in DMSO to a concentration of 10 mM, of which a small volume was diluted with binding buffer to the desired dilution. The assay plate was sealed, protected from light, and incubated for 2h at room temperature. The reaction wells were then vacuum filtered through 0.125% PEI-soaked PerkinElmer glass fiber filtermats followed by five washes with cold wash buffer (50 mM HEPES, pH 7.4). Filtermats were dried and 3H-naltrexone counts were measured via scintillation using MeltiLex B/HS wax scintillant on a PerkinElmer BetaMax scintillation counter. Results were analyzed on GraphPad Prism10, normalizing to the naloxone curve present on each plate and using the "on-site fit Ki" nonlinear regression equation. All values were derived from three independent experiments in triplicate and performed on different days.

BRET GI Activation Assay for α_{2A}

G protein activation by human α_{2A}AR was monitored with Gα_{i1}-RLucII[47] together with Gβ_1 and Gγ_2-GFP$_{10}$. In brief, HEK293T cells (gift from the Chair of Physiology, FAU Erlangen-Nürnberg) were transfected with 200 ng receptor plasmid (receptor:G$_\alpha$:G$_\beta$:Gγ ratio 2:0.5:1:4) using linear polyethylenimine (PEI, Polysciences, 3:1 PEI:DNA ratio). The DNA was complemented to a total amount of 1 μg DNA per $3 \cdot 10^5$ cells with ssDNA (Sigma-Aldrich) and 10,000 cells per well were transferred into 96-well half a rea plates (Greiner, Frickenhausen, Germany). 48 h after transfection, the cell medium was exchanged with PBS (phosphate buffered saline) and cells were stimulated with ligands at 37 °C for 10 min. Coelenterazine 400a (abcr GmbH, Karlsruhe, Germany) at a final concentration of 2.5 μM was added 5 min before measurement. BRET was monitored on a Clariostar plate reader (BMG, Ortenberg, Germany) with the appropriate filter sets (donor 410/80 nm, acceptor 515/30 nm) and was calculated as the ratio of acceptor emission to donor emission. BRET ratio was normalized to the effect of buffer (0%) and the maximum effect of norepinephrine (100%) and the obtained responses were analyzed using the equation for sigmoid concentration−response curves (four-parameter) implemented in GraphPad Prism 10 for Windows (GraphPad Software, La Jolla, USA) to derive the maximum effect (E_{max}, relative to norepinephrine) and the ligand potency (EC$_{50}$). For each compound two to four individual experiments were performed each done in duplicates.

GloSensor cAMP Assay for α_{2A} and MOR

The GloSensor cAMP assay was performed following the manufacturer's instructions (Promega) with slight modifications as previously described.[48,58] Briefly, wild-type (WT) human α_{2A} and MOR were cloned into the pcDNA3.1 vector and cotransfected with the 22F cAMP GloSensor plasmid into HEK293T cells cultured in 6-well plates. After 24 h, cells were reseeded into 96-well white plates in CO_2-independent medium and equilibrated with GloSensor cAMP reagent as per the manufacturer's protocol. Cells were incubated for 1 h at 37 °C followed by 1 h at room temperature. Where applicable, 10 μM forskolin was used to elevate basal cAMP levels for assessing receptor-mediated inhibition. Serially diluted test compounds were added and luminescence signals were recorded using a PerkinElmer microplate reader. Data were analyzed using GraphPad Prism 9.0 to calculate EC$_{50}$values.

DAT, NET and SERT Radioligand Binding

DAT, NET, and SERT activities were determined using a neurotransmitter transporter update assay kit from Molecular Devices (Category R8174). Briefly, HEK293 cells stably expressing human DAT, NET, or SERT were plated in Poly-L-Lys (PLL) coated 384-well black clear bottom plates in DMEM supplemented with 1% dialyzed FBS (dFBS) at a density of 15,000 cells in 40 μL per well. After overnight recovery, medium was removed and the cells were incubated with 25 ul/well drug solutions prepared in the assay buffer (1x HBSS, 20 mM HEPES, pH 7.4, supplemented with 1 mg/mL BSA) for 30 min at 37C, followed by 10 ul/well neurotransmitter dye solution (also prepared in the same assay buffer) for another 30 min at 37C. Cocaine, Nisoxetine, and fluoxetine served as positive controls for DAT, NET, and SERT, respectively. Fluorescence intensity was measured on the FlexStation II with excitation at 440 nm and emission at 520 nm. Relative fluorescence units (RLU) were exported and analyzed in Prism10.

GPCRome Screening

Off-target agonist activity at human GPCRome was carried out using the PRESTO-Tango assays as described[36,48] with modifications. HTLA cells were plated in PLL coated white clear-bottom 384-well plates in DMEM supplemented with 1% dFBS at a density of 10,000 cells in 40 μL per well. After recovery for about 6 h, the cells were transfected with 20 ng DNA per well for overnight incubation followed by addition of 10 μL of test compounds prepared in DMEM supplemented with 1% dFBS. The cells were incubated with compounds overnight (usually 16−20 h). Medium and drugs were then removed and 20 μL per well of BrightGlo reagents diluted in assay buffer were added. Plates were incubated for 20 min at room temperature in the dark and luminescence was counted. In each plate, the dopamine receptor D$_2$ was included as an assay control and was stimulated with 100 nM of the agonist quinpirole. Each receptor had 4 replicate wells of basal (with medium) and 4 replicate wells of sample (10 μM final in this case). Results were expressed in as fold change over average basal.

Expression and Purification of α_{2A} Adrenergic Receptor

The human wildtype α_{2A} was cloned to pVL1392 vector with an N-terminal FLAG tag for expression in Sf9 insect cells. Recombinant baculovirus was generated using the BestBac system. Sf9 cells were grown in ESF921 Medium (Expression Systems) and were infected with baculovirus at a density of ~4 × 106 cells/ml in the presence of 5 μM rauwolscine hydrochloride (Fisher Scientific). After 48 h of infection at 27 °C, the cells were harvested by centrifugation at 4000g for 20 min. Cell pellets were stored at −80 °C.

Thawed cell pellets from a 2 L SF9 expression harvest were resuspended in 400 mL hypotonic lysis buffer comprising 20 mM HEPES (pH 7.5), 1 mM EDTA, and a PierceTM Protease Inhibitor Tablet. Cell membranes were centrifuged at 38,000g for 15 min and solubilized with 40 mL buffer consisting of 20 mM HEPES (pH 7.5), 500 mM NaCl, 1% n-Dodecyl-b-D-Maltopyranoside (DDM)/0.1% Cholesteryl Hemisuccinate (CHS), 0.2% sodium cholate, 5 μM rauwolscine hydrochloride, and a PierceTM Protease Inhibitor Tablet in a dounce homogenizer. Resuspended membranes were then solubilized in a total of 200 mL solubilization buffer and stirred for 1 h. Insoluble debris was separated by centrifugation at 50,000g for 30 min. The supernatant was supplemented with 4 mM CaCl2 and mixed with 3 mL of homemade M1-Flag antibody-conjugated sepharose beads. Batch binding was carried out with gentle rotation at 4 °C for 2 h. The beads were spun down at 100g for 5 min and transferred to a gravity-flow column. Beads were washed with 40 mL wash buffer made up of 20 mM HEPES 7.5, 500 mM NaCl, 0.05% DDM/0.005% CHS, 2 mM CaCl2, 0.02% Sodium cholate, 10 uM **z7149**). Protein was eluted with 15 mL elution buffer comprising 20 mM HEPES 7.5, 100 mM NaCl, 0.05% DDM/0.005% CHS,0.02% sodium cholate, 10 uM z7149, 0.2 mg/mL Flag peptide, 5 mM EDTA) in 1 mL steps. Protein was then concentrated in a 50 kDa MWCO Amicon spin concentrator, and injected onto a Superdex200 Increase 10/300GL (Cytiva) gel filtration

https://doi.org/10.1021/acs.jmedchem.5c03810
J. Med. Chem. 2026, 69, 6210−6229

column equilibrated in 20 mM HEPES 7.5, 100 mM NaCl, 0.05% DDM/0.005% CHS, 0.02% sodium cholate, 10 uM **z7149** to isolate monodisperse material for further complexing with GαoGβ1γ2 heterotrimer, and scFv16.

Expression and Purification of GαoGβ1γ2 Heterotrimer

The human Gαo was cloned into pVL1392 vector while Gβ1 subunit with an N-terminal 6x His-tag, and untagged Gγ2 were cloned into a bicistronic pVLDual vector. The GαoGβ1γ2 was produced in HighFive insect cells grown in ESF921 medium (Expression systems). Cells at a density ~3 × 106 cells/ml were infected with Gαo and Gβ1γ2 baculovirus at a ratio 15 mL/lt. and 10 mL/lt. respectively. After 48 h of incubation, cells were harvested by centrifugation at 4000*g* for 20 min and stored in −80 °C. Cell pellets were thawed and resuspended in lysis buffer (200 mL buffer per liter of cell culture pellet) comprising of 10 mM HEPES pH 7.5, 0.1 mM MgCl2, 5 mM β-mercaptoethanol (β-ME), 10 μM guanosine diphosphate (GDP), and a PierceTM Protease Inhibitor Tablet. Cell membranes were centrifuged at 38,500*g* for 15 min. The pellet was resuspended in solubilization buffer (20 mM HEPES pH 7.5, 100 mM NaCl, 1% sodium cholate, 0.05% DDM, 5 mM MgCl2, 2 μL CIP (New England Biolabs), 5 mM β-ME, 20 mM imidazole, 10 μM GDP), and a PierceTM Protease Inhibitor Tablet using a Dounce homogenizer (200 mL buffer per liter of cell culture pellet). Resuspended membranes were then stirred for 30 min at 4 °C. To pellet insoluble debris, the solubilized membranes were centrifuged at 38,500*g* for 15 min. The supernatant was mixed with 8 mL Ni-NTA resin prewashed with solubilization buffer. To enable batch binding, solution was incubated for 2 h at 4 C with gentle rotation. Ni-NTA resin was collected by centrifugation at 500*g* for 10 min. Ni-NTA resin was washed twice with 40 mL solubilization buffer per wash. For slow exchange of protein into buffer without sodium cholate, Ni-NTA resin was transferred to a gravity-flow column and washed 5 times with 20 mL buffer each time. These washes contain the following ratios of E1 and E2 buffers: 50−50, 25−75, 10−90, 5−95, 0−100 where E1 was solubilization buffer supplemented with 5 mM Imidazole and E2 was 20 mM HEPES pH 7.50, 100 mM NaCl, 0.05% DDM, 1 mM MgCl2, 5 mM β-ME, 20 μM GDP, PierceTM Protease Inhibitor Tablet, and 20 mM Imidazole. A final wash in 25 mL of E2 buffer supplemented with 30 mM Imidazole was followed by elution using 40 mL of E2 buffer supplemented with 250 mM imidazole. Elution was incubated with 5 μL lambda phosphatase (supplemented with 1 mM MnCl2 for activity), 1 μL CIP (NEB), 1 uL Antarctic phosphatase, and incubated at 4 °C for 30 min with gentle rocking. The protein was then dialyzed using 10 kDa cutoff snakeskine membrane against in 1 L of dialysis buffer comprising 20 mM HEPES 7.5, 100 mM NaCl, 0.05% DDM, 1 mM MgCl2, 10 μM GDP, 100 μM TCEP for 16 h. Protein was supplemented with 5% Glycerol and 100 μM TCEP, and concentrated using a 50 kDa Amicon concentrator. The concentrated heterotrimeric GαoGβ1γ2 was aliquoted, flash frozen in liquid nitrogen, and stored at −80 °C.

Complex Formation of α_{2A} with GαoGβ1γ2 Heterotrimer and scFv16

Protein scFv16 was expressed and purified as previously reported.[82] Purified GαoGβ1γ2 heterotrimer was mixed with α_{2A} in a 1.5 molar excess, 1 μL apyrase (NEB), and 30 μM **z7149.** The complex was incubated at 4 °C for 16 h and then mixed with 0.5 mL homemade M1-Flag antibody-conjugated Sepharose beads, supplemented with 2 mM CaCl2. For slow detergent exchange of protein into LMNG buffer, beads were transferred to a gravity-flow column and washed 5 times with 10 mL buffer each time. These washes contain the following ratios of DDM and LMNG/GDN buffers: 50−50, 25−75, 10−90, 5−95, 0−100 where DDM buffer comprised of 20 mM HEPES 7.5, 100 mM NaCl, 0.05% DDM/0.005% CHS, 0.02% sodium cholate, 2 mM CaCl2, 10 μM z7149 and LMNG/GDN buffer was made of 20 mM Hepes 7.5, 100 mM NaCl, 0.0075% LMNG/0.0025%GDN/0.001%CHS, 2 mM CaCl2, 10 μM z7149. Protein was eluted using elution buffer 2 made of 20 mM HEPES pH 7.5, 100 mM NaCl, 0.0075% LMNG/0.0025% GDN/0.001%CHS, 10 μM **z7149**, 0.2 mg/mL Flag peptide, 5 mM EDTA). Protein was then concentrated in a 50 kDa MWCO Amicon spin concentrator and mixed with scFv16 in a 2.5 molar excess. After a 1 h incubation, the complex was injected onto a Superdex200 Increase 10/300GL (Cytiva) gel filtration column equilibrated in 20 mM HEPES 7.5, 100 mM NaCl, 0.00075% LMNG/0.00025%GDN/ 0.001%CHS, 10 μM **z7149**) to isolate monodisperse material for cryoEM grid preparation.

Expression and Purification of SERT and Reconstitution in Nanodiscs

Full- N- and C-terminally truncated (ΔN72/ΔC13) human wild-type SERT and Fab15B8 were expressed in Expi293 TetR cells as described previously.[36] On the day of purification, Expi293 cells were thawed and resuspended in lysis buffer comprised of 20 mM HEPES pH 7.50, 1 mM ethylenediaminetetraacetic acid (EDTA), EDTA-free protease inhibitor (Thermo Fisher), and 1 mM serotonin (5-HT). After stirring for 10 min, lysate was centrifuged at 14,000*g* for 10 min. The cell pellet was dounce homogenized into solubilization buffer comprised of 300 mM NaCl, 50 mM HEPES pH 7.50, 1.5% (w/v) n-dodecyl-β-D-maltoside (DDM), 0.1% (w/v) cholesteryl hemisuccinate (CHS), EDTA-free protease inhibitor (Thermo Fisher), and 3 mM 5-HT. Cells were solubilized for 60 min at 4 °C and centrifuged at 14,000*g* for 30 min at 4 °C. The supernatant was supplemented with 2 mM CaCl2 and loaded on homemade antiprotein C affinity resin. The resin was washed with 20 column volumes (C.V.) of buffer comprised of 150 mM NaCl, 20 mM HEPES pH 7.50, 0.1% (w/v) DDM, 0.01% (w/v) CHS, 2 mM CaCl2, and 3 mM 5-HT. SERT was eluted with 150 mM NaCl, 20 mM HEPES pH 7.50, 0.1% (w/v) DDM, 0.01% (w/v) CHS,, 3 mM 5-HT, 1 mM EDTA, and 0.2 mg/mL protein C peptide (Genscript). Monodisperse SERT was purified by size-exclusion chromatography (SEC) in buffer comprised of 50 mM NaCl, 20 mM HEPES pH 7.50, 0.1% (w/v) DDM, 0.01% (w/v) CHS, 1 mM 5-HT. SEC purified SERT was reconstituted into lipidic nanodiscs by mixing with purified MSPNW9[83] and a lipid mixture containing 2:3 weight ratio of 1-palmitoyl-2-oleoylphosphatidylcholine (POPC, Avanti) and 1-palmitoyl-2-oleoyl-*sn*-glycero-3-phospho-(10-rac-glycerol) (POPG, Avanti). A SERT:MSPNW9:lipid molar ratio of 1:20:400 was used in buffer containing 20 mM HEPES pH 7.50, 100 mM NaCl, 1 mM EDTA, 1 mM 5-HT. Samples were incubated under slow rotation for 1 h at 4 °C. Detergent was removed by addition of 300 mg SM-2 BioBeads (BioRad) followed by incubation under slow rotation for 16 h at 4 °C. The reconstituted sample was separated from BioBeads and 2 mM $CaCl_2$ was added before loading over on antiprotein C affinity resin. The resin was washed with 10 C.V. of 150 mM NaCl, 20 mM HEPES (pH 7.50), 1 mM CaCl, and nanodisc-SERT was eluted with 150 mM NaCl, 20 mM HEPES pH 7.50, 1 mM EDTA, and 0.2 mg/mL protein C peptide. The nanodisc-SERT sample was mixed with 1.5 fold molar excess of purified Fab15B8, and allowed to complex for 30 min on ice before SEC over a Superdex S200 Increase 10/300 GL column (GE Healthcare) into buffer comprised of 150 mM NaCl and 20 mM HEPES (pH 7.50). Fractions containing apo nanodisc-SERT-Fab15B8 sample were contcentrated on a 50k MWCO spin filter (Amicon), supplemented with 100 μM **z7149**, and incubated for 1 h on ice before cryoEM grid preparation.

Expression and Purification of MOR/'0505 Complex

Full-length, human MOR fused to a signal flag peptide at the N-terminus and a miniGo protein at the C-terminus was cloned into a pCDNA3.1-zeo-tetO plasmid. Expi293F inducible cells (ThermoFisher Scientific) maintained in Expi293F media with 50 μg/mL Blasticidin were transfected with this construct at a cell density of 2.5 × 106 by Expifectamine (ThermoFisher Scientific) following manufacturer instructions. Transfected cells were supplemented 24 h later with enhancers 1 and 2 from the transfection kit, 2 μg/mL doxycycline, and 1 μM Naloxone Hydrochloride. Cell pellets from a 200 mL culture were harvested 48 h post-transfection by centrifugation at 4000*g* for 20 min at 4 °C, weighed, and frozen at −80 °C until purification.

Cell pellets were thawed on the day of purification and resuspended for 15 min at 4 °C in lysis buffer consisting of 20 mM HEPES pH 7.5, 1 mM EDTA, 2 protease inhibitor cocktail tablets (ThermoFisher Scientific), and 35 μM of '0505. Resuspended cell pellets were

https://doi.org/10.1021/acs.jmedchem.5c03810
J. Med. Chem. 2026, 69, 6210−6229

centrifuged for 15 min at 14,000 rpm for 15 min at 4 °C (JA 25.50 rotor, Beckman Coulter) to collect the pelleted membrane fraction. Membranes were dounce-homogenized with ten strokes in a tight glass homogenizer and solubilized for 1 h at 4 °C with stirring in 20 mM HEPES pH 7.5, 150 mM NaCl, 1% Dodecyl Maltoside (DDM, Anatrace), 0.3% CHAPS, 0.1% CHS, 2 mM MgCl2, 5 mM ATP, 100 μM TCEP, 2 protease inhibitor cocktail tablets, and 35 μM '0505. Solubilized membranes were clarified by centrifugation at 14,000 rpm for 30 min at 4 °C in a JA 25.50 rotor, and then supplemented with CaCl2 to a concentration of 5 mM. and then batch-bound for 1 h at 4 °C with M1-FLAG resin equilibrated with ATP wash buffer consisting of 20 mM HEPES pH 7.5, 150 mM NaCl, 0.1% DDM, 0.01% CHS, 0.03% CHAPS, 2 mM CaCl2, 2 mM MgCl2, 5 mM ATP, 100 μM TCEP, and 35 μM '0505. Resin was collected by centrifugation for 5 min at 500 rpm (Sorvall Legend XTR, ThermoFisher Scientific), loaded onto a 2 mL Kimble Flex-Column and then washed with 10 CVs of ATP wash buffer. Slow detergent exchange occurred by washing the resin through a combination of low-DDM wash buffer (Buffer B: 20 mM HEPES pH 7.5, 150 mM NaCl, 0.1% DDM, 0.01% CHS, 0.03% CHAPS, 2 mM CaCl2, 100 μM TCEP, 35 μM '0505) and Glyco-Diosgenin (GDN)-exchange buffer (Buffer A: 20 mM HEPES pH 7.5, 150 mM NaCl, 0.2% GDN, 0.02% CHS, 2 mM CaCl2, 100 μM TCEP, 35 μM '0505). Exchange occurred by first washing the resin with 10 CVs of buffer B, 5 CVs of 1:1 buffer B:buffer A, 5 CVs of 3:1 buffer B:buffer A, 5 CVs of 7:1 buffer B:buffer A, and 2 CVs of buffer A. Resin was further washed with 10 CVs of low-GDN wash buffer consisting of 20 mM HEPES pH 7.5, 150 mM NaCl, 0.02% GDN, 0.002% CHS, 2 mM CaCl2, 100 μM TCEP, 35 μM '0505 and then eluted with 6 CVs of elution buffer consisting of 20 mM HEPES pH 7.5, 150 mM NaCl, 0.01% GDN, 0.001% CHS, 100 μM TCEP, 35 μM '0505, 5 mM EDTA, and 0.2 mg/mL FLAG peptide. Elution fractions were pooled and then concentrated with a 50 kDa cutoff Amicon concentrator. The concentrated MOR was injected into a Superose 6 10/300 GL sizing column equilibrated with SEC buffer 1 (20 mM HEPES pH 7.5, 150 mM NaCl, 0.01% GDN, 0.001% CHS, 100 μM TCEP, and 50 μM '0505). Monodisperse fractions were collected, pooled, and concentrated with a 50 kDa cutoff Amicon concentrator.

Purified Gβγ and scFv16 in 2-fold molar excess was precomplexed together in SEC buffer 1 and then complexed overnight with purified MOR on ice. The complex was injected the following day into a Superose 6 10/300 GL sizing column equilibrated with SEC buffer 2 (20 mM HEPES pH 7.5, 150 mM NaCl, 0.005% GDN, 0.0005% CHS, 100 μM TCEP, and 50 μM '0505). Monodisperse fractions were collected, concentrated to ∼3 mg/mL with a 100 kDa cutoff Amicon concentrator, and then immediately used for cryoEM sample preparation.

CryoEM Sample Preparation and Data Collection

300 mesh UltrAuFoil R 1.2/1.3 gold grids (Quantifoil) were glow-discharged in an EMS 700 Glow Discharge system (Electron Microscopy Sciences). Three μL of the α2AAR-GαoGβ1γ2-scFv16 complex, 2.75 μL of the nanodisc-SERT-Fab15B8 sample, and 4 μL of the MORminiGoNT- Gβ1γ2-scFv16 complex were separately applied to the grids in a Vitrobot Mark IV set at 4 °C with 100% humidity, blotted for 1.5−3 s (α2AAR and SERT) or 5−7 s (MOR) with a wait time of 10 s at a blot force of 0, then plunge-frozen into liquid ethane cooled at liquid nitrogen temperatures. Clipped grids were loaded into a 300 kV Titan Krios G2 microscope equipped with a BioQuantum energy filter set at 20 eV and a K3 direct electron detector camera. Details on data collection parameters and statistics are described in SI Table 3.

Cryo-EM Data Processing

Raw movies were motion corrected using MotionCor2 (10.1038/nmeth.4193) and resulting micrographs were imported into cryoSPARC v4.5.3 (Structura Biotechnology Inc.). Contrast transfer functions were calculated using Patch CTF estimation.

For α_{2A}AR, particles were picked using blob picker with a particle diameter range from 100 to 200 and an ab initio model was generated. This was used for template picking and 5,100,657 particles were extracted with a box size of 360 binned to 90 pixels. Particles were sorted with multiple rounds of 3D classification by heterogeneous refinement, using initial model as low pass filtered templates. Particles were subsequently unbinned and sorted by multiple rounds of ab initio reconstructions and heterogeneous refinements. 3D classification. Local refinement using a focus mask that covers the seven transmembrane domain of α_{2A}AR of the best class comprising of 38,025 particles yielded a 3.3 Å reconstruction.

For SERT, particles were template picked using a previously determined model.[36] A total of 2,859,480 particles were extracted with a 360 pixel box that was binned to 96 pixels and sorted by two rounds of 3D classification by heterogeneous refinement, using the initial model as a low pass filtered templates. Particles were unbinned and subjected to sorting by several rounds of two- and four-class ab initio reconstruction. 3D classification was performed with a focus mask of SERT and the variable chains of Fab15B8. Finally local refinement was performed on the resulting 9,815 particles with the same focus mask yielding a 3.4 Å map.

For MOR, micrograph denoising was carried out (greyscale normalization 0.8) followed by template picking using a 20 Å lowpass-filtered template (created from a ab initio model) at a diameter of 180 Å to extract 10,381,789 particles at a box size of 360 pixels binned to 90 pixels and subjected to heterogeneous refinement with 2 template classes and 4 noise classes. Template class particles were recollected and subjected to three more rounds of heterogeneous refinement with 2 template classes and 4 noise classes to clean the data set further. Particles were unbinned and subjected to sorting by several rounds heterogeneous refinement to yield 881,052 particles. A reference volume was created from this particle stack using nonuniform refinement, and the cryoSPARC particles file was exported and converted to a.star file using PyEM's csparc2star.py script (https://zenodo.org/records/3576630) and imported into RELION 4.0.1 (https://portlandpress.com/biochemj/article/478/24/4169/230248/New-tools-for-automated-cryo-EM-single-particle) along with the location information on the extracted particles. 3D classification with a reference mask was carried out to obtain 52,988 particles that had the best-resolved ligand density and exported back to cryoSPARC. This class was subjected to one more round of nonuniform refinement to produce a map at 3.32 Å and then locally refined using a TM-specific mask to produce a map at 3.34 Å.

CryoEM Model Building and Refinement

For α_{2A}AR, a starting model was generated from PDB 7EJ8 and fit into the cryoEM map using ChimeraX (10.1002/pro.3235). For SERT and MOR, initial models were generated from PDB 7MGW and 7T2G respectively. These were roughly fit using Chimera X and further refined using the ISOLDE plugin (https://journals.iucr.org/d/issues/2018/06/00/ic5101/index.html). Small molecule models and rotamer libraries were generated in eLBOW and the ligands were fit into maps using Coot. Models were subjected to multiple rounds of real-space refinement in Phenix, which was also used to perform final map-model validations.

Compound Preparation for *In Vivo* Studies

Both **Z7149** and '**0505** were synthesized by Enamine to better than 98% analytical purity (by LC/MS and ^{1}H NMR) and dissolved into their respective formulations (SI Figure 9) 30 min before testing. Both compounds were prepared in the captisol-water (4/6, v/v) vehicle. The molecules were dissolved in their trifluoroacetic acid salt forms to aid solubility.

Animals and Ethical Compliance

Animal experiments were approved by the UCSF Institutional Animal Care and Use Committee (IACUC) and the Duke University IACUC were conducted in accordance with the NIH Guide for the Care and Use of Laboratory animals (protocols no. AN181214 and A069−03−23 respectively). Adult (8 to 10 weeks old) male C56BL/6J mice (strain no. 000664) were purchased from the Jackson Laboratory. Mice were housed in cages on a standard 12:12 h light-dark cycle with food and water available *ad libitum*. At Duke University, 10−12 week-old male and female C57BL/6J (#000664; Jackson Laboratories, Bar Harbor, ME) and wild-type (WT) and vesicular monoamine transporter 2

https://doi.org/10.1021/acs.jmedchem.5c03810
J. Med. Chem. 2026, 69, 6210−6229

(VMAT2) heterozygous mice[38,69] were used. Mice were housed 3−4 per cage in a humidity- and temprature-controlled room on a 14:10 h (lights on at 0600 h) light-dark cycle and given chow and water *ad libitum*. The α_{2A} D79N mutant mice were purchased from Jackson (stock no. 2777), and 7- to 8-week-old females were used. Sample sizes were modeled on our previous studies and on studies using a similar approach, which were able to detect significant changes (96, 97). The animals were randomly assigned to treatment and control groups. Animals were initially placed into one cage and allowed to freely run for a few minutes. Then each animal was randomly picked up, injected with compound treatment or vehicle, and placed into a separate cylinder before the behavioral test.

Pharmacokinetics

Pharmacokinetics were measured by Bienta (Enamine Biology Services) in accordance with Enamine pharmacokinetic study protocols and Institutional Animal Care and Use Guidelines (protocol number 1−2/2020). Plasma pharmacokinetics, brain distribution and CSF distribution for six polypharmacology ligands (SI Table 1) were measured after a 10 mg/kg (i.p.) dose. In each study, nine time points (5, 15, 30, 60, 120, 240, 360, 480, and 1440 min) were collected, with each of the time point measured from three animals. There was also a control group of one animal. For all compound studies the animals were randomly assigned to the treatment groups before the pharmacokinetic study; all animals were fasted for 4 h before dosing.

Mice were injected (i.p.) with 2,2,2- tribromoethanol at 150 mg/kg before drawing CSF and blood. The CSF was collected under a stereomicroscope from the cisterna magna using 1 mL syringes. Blood collection was performed from the orbital sinus into microtainers containing K3EDTA. Animals were euthanized by cervical dislocation after the blood samples collection. Blood samples were centrifuged for 10 min at 3000 rpm. Brain samples (right lobe) were weighed and transferred into 1.5 mL tubes. All samples were immediately processed, flash-frozen and stored at −70 °C until subsequent analysis.

Plasma samples (40 mL) were mixed with 200 mL of internal standard (IS) solution. After mixing by pipetting and centrifuging for 4 min at 6000 rpm, 4 mL of each supernatant was injected into the liquid chromatography−tandem mass spectrometry (LC-MS/MS) system. Solutions of internal standards were used to quantify compounds in the plasma samples. Brain samples (weight 200 ± 1 mg) were homogenized with 800 mL of an internal stock solution using zirconium oxide beads (115 ± 5 mg) in a Bullet Blender homogenizer for 30 s at speed 8. After this, the samples were centrifuged for 4 min at 14,000 rpm, and supernatant was injected into LC-MS/MS system. CSF samples (2 mL) were mixed with 40 mL of an internal stock solution. After mixing by pipetting and centrifuging for 4 min at 6000 rpm, 5 mL of each supernatant was injected into LC-MS/MS system.

The concentrations of compounds in plasma and brain samples were determined using HPLC-MS/MS. Data acquisition and system control were performed using Analyst 1.5.2 software (AB Sciex, Canada). The concentrations of the test com- pound below the lower limit of quantitation (LLOQ = 10 ng/mL for plasma, 20 ng/g for brain, and 5 ng/mL for CSF samples) were designated as zero. Pharmacokinetic data analysis was performed using noncompartmental, bolus injection or extravascular input analysis models in WinNonlin 5.2 (PharSight). Data below LLOQ were presented as missing to improve validity of $T_{1/2}$ calculations.

Nociceptive Analyses

For all behavioral tests, the experimenter was always blind to treatment. Animals were first habituated for 1 h in Plexiglas cylinders and then tested 30 min after IP compound injection. Mechanical (von Frey), thermal (Hargreaves, hot plate, and tail flick) and ambulatory (rotarod) tests were conducted as described.[84] Hindpaw mechanical thresholds were measured with von Frey filaments using the up−down method.[85] Hindpaw thermal sensitivity was measured with a radiant heat source (Hargreaves) or a 52 °C hot plate. For the tail flick assay, sensitivity was measured by immersing the tail into a 50 °C water bath for both WT and D79N mutant mice. For the ambulatory (rotarod) test, mice were first trained on an accelerating rotating rod, 3 times for 5 min, before testing with any compound.

SNI Model of Neuropathic Pain

Under isoflurane anesthesia, two of the three branches of the sciatic nerve were ligated and transected, leaving the sural nerve intact. Behavior was tested 7 to 14 days after injury.

CFA

The CFA model of chronic inflammation was induced as described previously.[86] Briefly, CFA (Sigma) was diluted 1:1 with saline and vortexed for 30 min. When fully suspended, we injected 20 μL of CFA into one hindpaw. Heat withdrawal was measured before the injection (baseline) and 3 days after using the Hargreaves test.

4-Plate Assay

C57 BL/6J mice were used in these studies. The 4-plate assay was conducted using the apparatus with shocker for mice (Data Sciences International, St. Paul, MN) as described.[87] Mice were IP injected with vehicle (Veh; *N*,*N*-dimethyllacetamide, final volume 0.5%; Sigma-Aldrich) that was brought to volume with 5% 2-hydroxypropoyl-β-cyclodextrin (Sigma-Aldrich) in water (Mediatech Inc., Manassas, VA),0.5 mg/kg diazepam (DIAZ, #D0899; Sigma-Aldrich, St. Louis, MO) or 0.1, 0.17, or 0.25 mg/kg **Z7149**. Thirty min later a mouse was placed into the apparatus and given 30 s of nonpunished exploration time. Thereafter, when the animal began to move from a plate by placing two paws onto an adjacent plate, it received a foot-shock (0.4 mA for 0.5 s) as punishment. This event was followed by a 3 s time-out when crossings were not punished. The total numbers of nonpunished crossing (baseline) over 30 s and punished crossings over 120 s were recorded.

Tail Suspension Assay

VMAT2 mice were used in these experiments.[38,69] WT mice received the Veh, while VMAT2-HET mice were given Veh, 20 mg/kg fluoxetine-HCl (FLX, #0927; Tocris Biosciences, Bristol, UK), or 0.2 or 0.5 mg/kg of **Z7149**. Animals were tested acutely (30 min), 1, 3, and 5 days later in tail suspension over 6 min on each occasion. In the test, mice were suspended by their tails (connected to a load cell) in a Med Associates (St. Albans, VT) tail suspension apparatus. The signal from the load cell was processed with Med-Associates Tail Suspension Software for immobility times. All load cells were calibrated prior to testing each day according to the manufacturer's instructions.

Statistics

All statistical analyses for the animal studies were performed with IBM SPSS Statistics 29 programs (IBM, Chicago, IL). The data are presented as means and standard errors of the mean. No sex effects were detected and so this variable was collapsed. The 4-plate and tail suspension data were analyzed by repeated-measures ANOVA (RMANOVA), followed by Bonferroni corrected pairwise comparisons. Since Levene's test for homogeneity of variance was violated in the 4-plate test with C57BL/6J mice and in the tail suspension test with WT mice, Greenhouse-Geisser corrections were applied in the RMANOVA. A $p < 0.05$ was considered significant. All results were plotted using GraphPad Prism10.4.1 and the statistics are displayed in SI Table 2.

■ ASSOCIATED CONTENT

Data Availability Statement

CryoEM structures and data are available from the PDB via structure IDs: 9PNS/EMD-71770 (Z7149-SERT), 9PPQ/EMD-71775 (0505-MOR), and 9PQD/EMD-71783 (Z7149-α_{2A}). The authors will release the atomic coordinates upon article publication. Almost all other primary data is available from the SI of this paper, and otherwise available from the authors. The docking code is freely available for noncommercial use at https://dock.compbio.ucsf.edu.

Supporting Information

The Supporting Information is available free of charge at https://pubs.acs.org/doi/10.1021/acs.jmedchem.5c03810.

https://doi.org/10.1021/acs.jmedchem.5c03810
J. Med. Chem. 2026, 69, 6210−6229

List of likely dual-target ligands from retrospective docking (XLSX)

Table showing PK results for selected compounds. Figures showing retrospective docking results. Concentration−response curve for all molecules active on target and synthetic routes for the same. ^{1}H NMR and LC/MS spectra for the active molecules (PDF)

Compounds purchased and tested in this study (CSV)

AUTHOR INFORMATION

Corresponding Authors

Christian Billesboelle − *Department of Pharmaceutical Chemistry, University of California, San Francisco, San Francisco, California 94158, United States*; Email: Christian.Billesboelle@ucsf.edu

Bryan L. Roth − *Department of Pharmacology, University of North Carolina at Chapel Hill, Chapel Hill, North Carolina 27599-7365, United States*; orcid.org/0000-0002-0561-6520; Email: bryan_roth@med.unc.edu

Allan I. Basbaum − *Department of Anatomy, University of California, San Francisco, San Francisco, California 94158, United States*; Email: Allan.Basbaum@ucsf.edu

Aashish Manglik − *Department of Anesthesia and Perioperative Care, University of California, San Francisco, San Francisco, California 94158, United States*; Email: Aashish.manglik@ucsf.edu

William C. Wetsel − *Departments of Psychiatry and Behavioral Sciences, Neurobiology, and Cell Biology, Duke University Medical Center, Durham, North Carolina 27710, United States*; Email: william.wetsel@duke.edu

Brian K. Shoichet − *Department of Pharmaceutical Chemistry, University of California, San Francisco, San Francisco, California 94158, United States*; orcid.org/0000-0002-6098-7367; Phone: 415-531-4568; Email: bshoichet@gmail.com

Authors

Yujin Wu − *Department of Pharmaceutical Chemistry, University of California, San Francisco, San Francisco, California 94158, United States*

Seth Vigneron − *Department of Pharmaceutical Chemistry, University of California, San Francisco, San Francisco, California 94158, United States*

Joao Braz − *Department of Anatomy, University of California, San Francisco, San Francisco, California 94158, United States*

Karthik Srinivasan − *Department of Pharmaceutical Chemistry, University of California, San Francisco, San Francisco, California 94158, United States*; orcid.org/0000-0002-0457-5122

Elissa A. Fink − *Department of Pharmaceutical Chemistry, University of California, San Francisco, San Francisco, California 94158, United States*; orcid.org/0000-0001-5531-1971

Xi-Ping Huang − *Department of Pharmacology, University of North Carolina at Chapel Hill, Chapel Hill, North Carolina 27599-7365, United States*

Xinyu Xu − *Department of Pharmaceutical Chemistry, University of California, San Francisco, San Francisco, California 94158, United States*

Harald Huebner − *Department of Chemistry and Pharmacy, Friedrich-Alexander-Universität Erlangen-Nürnberg, Erlangen 91058, Germany*; orcid.org/0000-0002-7892-599X

Joseph Y. Kim − *Department of Pharmaceutical Chemistry, University of California, San Francisco, San Francisco, California 94158, United States*; orcid.org/0000-0002-6816-5958

Jing Wang − *Department of Pharmacology, University of North Carolina at Chapel Hill, Chapel Hill, North Carolina 27599-7365, United States*

Tara Pfeiffer − *Department of Chemistry and Pharmacy, Friedrich-Alexander-Universität Erlangen-Nürnberg, Erlangen 91058, Germany*; orcid.org/0000-0003-1701-0996

Kensuke Sakamoto − *Department of Pharmacology, University of North Carolina at Chapel Hill, Chapel Hill, North Carolina 27599-7365, United States*; orcid.org/0000-0003-4488-1244

Dmytro S. Radchenko − *Enamine Ltd., Kyiv 02094, Ukraine*; orcid.org/0000-0001-5444-7754

Ramona M. Rodriguiz − *Departments of Psychiatry and Behavioral Sciences, Neurobiology, and Cell Biology, Duke University Medical Center, Durham, North Carolina 27710, United States*

Yurii S. Moroz − *Enamine Ltd., Kyiv 02094, Ukraine; National Taras Shevchenko University of Kyiv, Kyiv 01601, Ukraine; Chemspace LLC, Kyiv 02094, Ukraine*; orcid.org/0000-0001-6073-002X

John J. Irwin − *Department of Pharmaceutical Chemistry, University of California, San Francisco, San Francisco, California 94158, United States*

Peter Gmeiner − *Department of Chemistry and Pharmacy, Friedrich-Alexander-Universität Erlangen-Nürnberg, Erlangen 91058, Germany*; orcid.org/0000-0002-4127-197X

Complete contact information is available at: https://pubs.acs.org/10.1021/acs.jmedchem.5c03810

Author Contributions

[†]Y.W., S.V., J.B., and K.S. contributed equally.

Author Contributions

B.K.S., Y.W., and E.A.F. designed the project. Y.W. and E.A performed the retrospective docking and Y.W. performed the prospective docking. Y.W. was responsible for the compound optimization, with input from B.K.S. S.V. tested compounds against the MOR. X.X., H.H., and T.P. (overseen by P.G.) tested molecules against the α_{2A} receptor. X.H. and J.W. tested molecules against SERT, NET, and DAT (overseen by B.L.R). X.H. and K.S. performed off-target screening (GPCRome). J.B. performed the nociceptive analysis with guidance from A.B. K.S. cloned, expressed, purified, collected cryoEM data, and conducted model building of the α_{2A} receptor. C.B.B. performed cloning, expression, purification, cryoEM data collection, data processing, and model building of SERT. J.Y.K. performed cloning, expression, purification, cryoEM data collection, data processing, and model building of MOR. A.M. oversaw the cryo-EM structure determination. R.M.R. conducted the 4-plate assay for anxiety-like behavior, analyzed the observations, and graphed the results for this and the tail suspension test. W.C.W. oversaw the behavioral experiments, organized the statistical results, wrote the Materials and Methods and Results sections for the 4-plate and tail suspension assays, and edited the manuscript. D.S.R. was responsible for compound synthesis and QC analysis, which Y.S.M. oversaw. J.J.I. provided support for large-scale docking. Y.W. and B.K.S. drafted and edited the manuscript. B.K.S. supervised the project. All authors reviewed and approved the final manuscript.

https://doi.org/10.1021/acs.jmedchem.5c03810
J. Med. Chem. 2026, 69, 6210−6229

Funding

This work is supported by DARPA grant HR0011-19-2-0020 (to B.K.S., A.M., A.I.B., and B.L.R.) and by NIH grant R35GM122481 (to B.K.S.).

Notes

The authors declare the following competing financial interest(s): B.K.S. is co-founder of Epiodyne, BlueDolphin, and Deep Apple Therapeutics, and serves on SAB for Schrodinger LLC, Vilya Therapeutics, Frontier Discovery Ltd, and on the SRB of Genentech. B.L.R.: is an SAB member for Septerna, Epiodyne, Lassogen, and ImprintBio, and is a co-founder of Epiodyne and ImprintBio. A.I.B is on the SABs of Neurona Therapeutics and Rapport Therapeutics. The remaining authors declare no competing interest.

■ ABBREVIATION USED

α2A: Alpha-2A adrenergic receptor (α2A)
MOR: μ-opioid receptor
SERT: Serotonin transporter

■ REFERENCES

(1) Błaszczyk, B.; Miziak, B.; Czuczwar, P.; Wierzchowska-Cioch, E.; Pluta, R.; Czuczwar, S. J. A viewpoint on rational and irrational fixed-drug combinations. *Expert review of clinical pharmacology* **2018**, *11* (8), 761−771.

(2) Gautam, C. S.; Saha, L. Fixed dose drug combinations (FDCs): rational or irrational: a view point. *British journal of clinical pharmacology* **2008**, *65* (5), 795.

(3) Hao, J.; Rodriguez-Monguio, R.; Seoane-Vazquez, E. Fixed-dose combination drug approvals, patents and market exclusivities compared to single active ingredient pharmaceuticals. *PloS one* **2015**, *10* (10), No. e0140708.

(4) Anighoro, A.; Bajorath, J.; Rastelli, G. Polypharmacology: challenges and opportunities in drug discovery: miniperspective. *Journal of medicinal chemistry* **2014**, *57* (19), 7874−7887.

(5) Roth, B. L.; Sheffler, D. J.; Kroeze, W. K. Magic shotguns versus magic bullets: selectively non-selective drugs for mood disorders and schizophrenia. *Nat. Rev. Drug Discovery* **2004**, *3* (4), 353−359.

(6) Li, N.; Li, C.; Han, R.; Wang, Y.; Yang, M.; Wang, H.; Tian, J. LPM580098, a novel triple reuptake inhibitor of serotonin, noradrenaline, and dopamine, attenuates neuropathic pain. *Front. Pharmacol.* **2019**, *10*, 53.

(7) Rastogi, A.; Jude, E. Novel treatment modalities for painful diabetic neuropathy. *Diabetes & Metabolic Syndrome: Clinical Research & Reviews* **2021**, *15* (1), 287−293.

(8) Apsel, B.; Blair, J. A.; Gonzalez, B.; Nazif, T. M.; Feldman, M. E.; Aizenstein, B.; Hoffman, R.; Williams, R. L.; Shokat, K. M.; Knight, Z. A. Targeted polypharmacology: discovery of dual inhibitors of tyrosine and phosphoinositide kinases. *Nat. Chem. Biol.* **2008**, *4* (11), 691.

(9) Dar, A. C.; Das, T. K.; Shokat, K. M.; Cagan, R. L. Chemical genetic discovery of targets and anti-targets for cancer polypharmacology. *Nature* **2012**, *486* (7401), 80−84.

(10) Willard, F. S.; Douros, J. D.; Gabe, M. B. N.; Showalter, A. D.; Wainscott, D. B.; Suter, T. M.; Capozzi, M. E.; van der Velden, W. J. C.; Stutsman, C.; Cardona, G. R.; Urva, S.; Emmerson, P. J.; Holst, J. J.; D'Alessio, D. A.; Coghlan, M. P.; Rosenkilde, M. M.; Campbell, J. E.; Sloop, K. W. Tirzepatide is an imbalanced and biased dual GIP and GLP-1 receptor agonist. *JCI insight* **2020**, *5* (17), No. e140532.

(11) Chavda, V. P.; Ajabiya, J.; Teli, D.; Bojarska, J.; Apostolopoulos, V. Tirzepatide, a new era of dual-targeted treatment for diabetes and obesity: a mini-review. *Molecules* **2022**, *27* (13), 4315.

(12) Liu, Q. K. Mechanisms of action and therapeutic applications of GLP-1 and dual GIP/GLP-1 receptor agonists. *Front. Endocrinol.* **2024**, *15*, No. 1431292.

(13) Besnard, J.; Ruda, G. F.; Setola, V.; Abecassis, K.; Rodriguiz, R. M.; Huang, X. P.; Norval, S.; Sassano, M. F.; Shin, A. I.; Webster, L. A.; Simeons, F. R. C.; Stojanovski, L.; Prat, A.; Seidah, N. G.; Constam, D. B.; Bickerton, G. R.; Read, K. D.; Wetsel, W. C.; Gilbert, I. H.; Roth, B. L.; Hopkins, A. L. Automated design of ligands to polypharmacological profiles. *Nature* **2012**, *492* (7428), 215−220.

(14) Blanchette, F.; Neuhaus, O. Glatiramer acetate: evidence for a dual mechanism of action. *Journal of neurology* **2008**, *255*, 26−36.

(15) Harvey, A. T.; Rudolph, R. L.; Preskorn, S. H. Evidence of the dual mechanisms of action of venlafaxine. *Archives of General Psychiatry* **2000**, *57* (5), 503−509.

(16) Mohamed, L. A.; Keller, J. N.; Kaddoumi, A. Role of P-glycoprotein in mediating rivastigmine effect on amyloid-β brain load and related pathology in Alzheimer's disease mouse model. *Biochimica et Biophysica Acta (BBA)-Molecular Basis of Disease* **2016**, *1862* (4), 778−787.

(17) Parvathaneni, V.; Kulkarni, N. S.; Muth, A.; Gupta, V. Drug repurposing: a promising tool to accelerate the drug discovery process. *Drug discovery today* **2019**, *24* (10), 2076−2085.

(18) Pushpakom, S.; Iorio, F.; Eyers, P. A.; Escott, K. J.; Hopper, S.; Wells, A.; Doig, A.; Guilliams, T.; Latimer, J.; McNamee, C.; Norris, A.; Sanseau, P.; Cavalla, D.; Pirmohamed, M. Drug repurposing: progress, challenges and recommendations. *Nat. Rev. Drug Discovery* **2019**, *18* (1), 41−58.

(19) Singh, T. U.; Parida, S.; Lingaraju, M. C.; Kesavan, M.; Kumar, D.; Singh, R. K. Drug repurposing approach to fight COVID-19. *Pharmacological reports* **2020**, *72*, 1479−1508.

(20) Sleire, L.; Førde, H. E.; Netland, I. A.; Leiss, L.; Skeie, B. S.; Enger, P. Ø. Drug repurposing in cancer. *Pharmacol. Res.* **2017**, *124*, 74−91.

(21) Blaschke, T.; Bajorath, J. Fine-tuning of a generative neural network for designing multi-target compounds. *J. Comput.-Aided Mol. Design* **2021**, 363.

(22) Brunetti, L.; Leuci, R.; Carrieri, A.; Catto, M.; Occhineri, S.; Vinci, G.; Gambacorta, L.; Baltrukevich, H.; Chaves, S.; Laghezza, A.; Altomare, C. D.; Tortorella, P.; Santos, M. A.; Loiodice, F.; Piemontese, L. Structure-based design of novel donepezil-like hybrids for a multi-target approach to the therapy of Alzheimer's disease. *Eur. J. Med. Chem.* **2022**, *237*, No. 114358.

(23) Chen, Z.; Wu, Y.; Liu, Y.; Yang, S.; Chen, Y.; Lai, L. Discovery of dual target inhibitors against cyclooxygenases and leukotriene A4 hydrolyase. *Journal of medicinal chemistry* **2011**, *54* (10), 3650−3660.

(24) Chen, Z.; Yu, J.; Wang, H.; Xu, P.; Fan, L.; Sun, F.; Huang, S.; Zhang, P.; Huang, H.; Gu, S.; Zhang, B.; Zhou, Y.; Wan, X.; Pei, G.; Xu, H. E.; Cheng, J.; Wang, S. Flexible scaffold-based cheminformatics approach for polypharmacological drug design. *Cell* **2024**, *187* (9), 2194−2208.

(25) Li, S.; Li, X.; Ma, L.; Luo, Z.; Yin, F.; Zhang, Y.; Chen, Y.; Wan, S.; Zhou, H.; Wang, X.; Kong, L. Polypharmacological Drug Design Guided by Integrating Phenotypic and Restricted Fragment Docking Strategies. *J. Med. Chem.* **2024**, 21049.

(26) Mouysset, B.; Le Grand, M.; Camoin, L.; Pasquier, E. Polypharmacology of existing drugs: How to crack the code? *Cancer Letters* **2024**, *588*, No. 216800.

(27) Ramsay, R. R.; Popovic-Nikolic, M. R.; Nikolic, K.; Uliassi, E.; Bolognesi, M. L. A perspective on multi-target drug discovery and design for complex diseases. *Clin. Transl. Med.* **2018**, *7*, 1−14.

(28) Shang, E.; Yuan, Y.; Chen, X.; Liu, Y.; Pei, J.; Lai, L. De novo design of multitarget ligands with an iterative fragment-growing strategy. *J. Chem. Inf. Model.* **2014**, *54* (4), 1235−1241.

(29) Wei, D.; Jiang, X.; Zhou, L.; Chen, J.; Chen, Z.; He, C.; Yang, K.; Liu, Y.; Pei, J.; Lai, L. Discovery of multitarget inhibitors by combining molecular docking with common pharmacophore matching. *Journal of medicinal chemistry* **2008**, *51* (24), 7882−7888.

(30) Yuan, Y.; Pei, J.; Lai, L. Ligbuilder v3: a multi-target de novo drug design approach. *Front. Chem.* **2020**, *8*, 142.

(31) Zhang, P.; Xu, S.; Zhu, Z.; Xu, J. Multi-target design strategies for the improved treatment of Alzheimer's disease. *European journal of medicinal chemistry* **2019**, *176*, 228−247.

https://doi.org/10.1021/acs.jmedchem.5c03810
J. Med. Chem. 2026, 69, 6210−6229

(32) Zhang, W.; Bai, Y.; Wang, Y.; Xiao, W. Polypharmacology in drug discovery: a review from systems pharmacology perspective. *Current pharmaceutical design* **2016**, *22* (21), 3171−3181.
(33) Zhou, S.; Li, Y.; Hou, T. Feasibility of using molecular docking-based virtual screening for searching dual target kinase inhibitors. *J. Chem. Inf. Model.* **2013**, *53* (4), 982−996.
(34) Weiss, D. R.; Ahn, S.; Sassano, M. F.; Kleist, A.; Zhu, X.; Strachan, R.; Roth, B. L.; Lefkowitz, R. J.; Shoichet, B. K. Conformation guides molecular efficacy in docking screens of activated β-2 adrenergic G protein coupled receptor. *ACS Chem. Biol.* **2013**, *8* (5), 1018−1026.
(35) Vigneron, S. F.; Ohno, S.; Braz, J.; Kim, J. Y.; Kweon, O. S.; Webb, C.; Billesbølle, C.; Bhardwaj, K.; Irwin, J.; Manglik, A. Docking 14 million virtual isoquinuclidines against the mu and kappa opioid receptors reveals dual antagonists-inverse agonists with reduced withdrawal effects. *ACS Cent. Sci.* **2025**, 770−790.
(36) Singh, I.; Seth, A.; Billesbølle, C. B.; Braz, J.; Rodriguiz, R. M.; Roy, K.; Bekele, B.; Craik, V.; Huang, X. P.; Boytsov, D.; Pogorelov, V. M.; Lak, P.; O'Donnell, H.; Sandtner, W.; Irwin, J. J.; Roth, B. L.; Basbaum, A. I.; Wetsel, W. C.; Manglik, A.; Shoichet, B. K.; Rudnick, G. Structure-based discovery of conformationally selective inhibitors of the serotonin transporter. *Cell* **2023**, *186* (10), 2160−2175.
(37) Manglik, A.; Lin, H.; Aryal, D. K.; McCorvy, J. D.; Dengler, D.; Corder, G.; Levit, A.; Kling, R. C.; Bernat, V.; Hübner, H.; Huang, X. P.; Sassano, M. F.; Giguère, P. M.; Löber, S.; Duan, D.; Scherrer, G.; Kobilka, B. K.; Gmeiner, P.; Roth, B. L.; Shoichet, B. K. Structure-based discovery of opioid analgesics with reduced side effects. *Nature* **2016**, *537* (7619), 185−190.
(38) Kaplan, A. L.; Confair, D. N.; Kim, K.; Barros-Álvarez, X.; Rodriguiz, R. M.; Yang, Y.; Kweon, O. S.; Che, T.; McCorvy, J. D.; Kamber, D. N.; Phelan, J. P.; Martins, L. C.; Pogorelov, V. M.; DiBerto, J. F.; Slocum, S. T.; Huang, X. P.; Kumar, J. M.; Robertson, M. J.; Panova, O.; Seven, A. B.; Wetsel, A. Q.; Wetsel, W. C.; Irwin, J. J.; Skiniotis, G.; Shoichet, B. K.; Roth, B. L.; Ellman, J. A. Bespoke library docking for 5-HT2A receptor agonists with antidepressant activity. *Nature* **2022**, *610* (7932), 582−591.
(39) Lyu, J.; Kapolka, N.; Gumpper, R.; Alon, A.; Wang, L.; Jain, M. K.; Barros-Álvarez, X.; Sakamoto, K.; Kim, Y.; DiBerto, J. AlphaFold2 structures guide prospective ligand discovery. *Science* **2024**, No. eadn6354.
(40) Tingle, B. I.; Tang, K. G.; Castanon, M.; Gutierrez, J. J.; Khurelbaatar, M.; Dandarchuluun, C.; Moroz, Y. S.; Irwin, J. J. ZINC-22— A free multi-billion-scale database of tangible compounds for ligand discovery. *J. Chem. Inf. Model.* **2023**, *63* (4), 1166−1176.
(41) Lyu, J.; Wang, S.; Balius, T. E.; Singh, I.; Levit, A.; Moroz, Y. S.; O'Meara, M. J.; Che, T.; Algaa, E.; Tolmachova, K.; Tolmachev, A. A.; Shoichet, B. K.; Roth, B. L.; Irwin, J. J. Ultra-large library docking for discovering new chemotypes. *Nature* **2019**, *566* (7743), 224−229.
(42) Chan, A. K. M.; Cheung, C. W.; Chong, Y. K. Alpha-2 agonists in acute pain management. *Expert opinion on pharmacotherapy* **2010**, *11* (17), 2849−2868.
(43) Giovannitti, J. A., Jr; Thoms, S. M.; Crawford, J. J. Alpha-2 adrenergic receptor agonists: a review of current clinical applications. *Anesthesia progress* **2015**, *62* (1), 31.
(44) Hayashi, Y.; Maze, M. Alpha2 adrenoceptor agonists and anaesthesia. *BJA: British Journal of Anaesthesia* **1993**, *71* (1), 108−118.
(45) Madariaga-Mazón, A.; Marmolejo-Valencia, A. F.; Li, Y.; Toll, L.; Houghten, R. A.; Martinez-Mayorga, K. Mu-Opioid receptor biased ligands: A safer and painless discovery of analgesics? *Drug discovery today* **2017**, *22* (11), 1719−1729.
(46) Pasternak, G. W. Molecular biology of opioid analgesia. *Journal of pain and symptom management* **2005**, *29* (5), 2−9.
(47) Siuda, E. R.; Carr, R., III; Rominger, D. H.; Violin, J. D. Biased mu-opioid receptor ligands: a promising new generation of pain therapeutics. *Current opinion in pharmacology* **2017**, *32*, 77−84.
(48) Fink, E. A.; Xu, J.; Hübner, H.; Braz, J. M.; Seemann, P.; Avet, C.; Craik, V.; Weikert, D.; Schmidt, M. F.; Webb, C. M.; Tolmachova, N. A.; Moroz, Y. S.; Huang, X. P.; Kalyanaraman, C.; Gahbauer, S.; Chen, G.; Liu, Z.; Jacobson, M. P.; Irwin, J. J.; Bouvier, M.; Du, Y.; Shoichet, B. K.; Basbaum, A. I.; Gmeiner, P. Structure-based discovery of nonopioid analgesics acting through the α2A-adrenergic receptor. *Science* **2022**, *377* (6614), No. eabn7065.
(49) Chabot-Doré, A. J.; Schuster, D.; Stone, L.; Wilcox, G. Analgesic synergy between opioid and α2-adrenoceptors. *British journal of pharmacology* **2015**, *172* (2), 388−402.
(50) Smith, H. Combination opioid analgesics. *Pain physician* **2008**, *11* (2), 201.
(51) Root-Bernstein, R. Adrenergic agonists and antagonists enhance opioid receptor activity. In *The Neurobiology, Physiology, and Psychology of Pain*; Elsevier, 2022; pp 79−89.
(52) Obata, H. Analgesic mechanisms of antidepressants for neuropathic pain. *International journal of molecular sciences* **2017**, *18* (11), 2483.
(53) Sawynok, J.; Esser, M. J.; Reid, A. R. Antidepressants as analgesics: an overview of central and peripheral mechanisms of action. *J. Psychiatry Neurosci.* **2001**, *26* (1), 21.
(54) Dharmshaktu, P.; Tayal, V.; Kalra, B. S. Efficacy of antidepressants as analgesics: a review. *Journal of Clinical Pharmacology* **2012**, *52* (1), 6−17.
(55) Smith, A. J. The analgesic effects of selective serotonin reuptake inhibitors. *Journal of Psychopharmacology* **1998**, *12* (4), 407−413.
(56) Patetsos, E.; Horjales-Araujo, E. Treating chronic pain with SSRIs: what do we know? *Pain Res. Manage.* **2016**, *2016* (1), 1.
(57) Barkin, R. L.; Fawcett, J. The management challenges of chronic pain: the role of antidepressants. *American journal of therapeutics* **2000**, *7* (1), 31−49.
(58) Vigneron, S. F.; Ohno, S.; Braz, J.; Kim, J. Y.; Kweon, O. S.; Webb, C.; Billesbølle, C. B.; Srinivasan, K.; Bhardwaj, K.; Irwin, J. J.; Manglik, A.; Basbaum, A. I.; Ellman, J. A.; Shoichet, B. K. Docking 14 Million Virtual Isoquinuclidines against the μ and κ Opioid Receptors Reveals Dual Antagonists−Inverse Agonists with Reduced Withdrawal Effects. *ACS Central Science* **2025**, *11* (5), 770−790.
(59) Liu, F.; Mailhot, O.; Glenn, I. S.; Vigneron, S. F.; Bassim, V.; Xu, X.; Fonseca-Valencia, K.; Smith, M. S.; Radchenko, D. S.; Fraser, J. S. The impact of library size and scale of testing on virtual screening. *Nat. Chem. Biol.* **2025**, 1−7.
(60) Lyu, J.; Irwin, J. J.; Shoichet, B. K. Modeling the expansion of virtual screening libraries. *Nat. Chem. Biol.* **2023**, *19* (6), 712−718.
(61) Abbott, F.; Hong, Y.; Blier, P. Activation of 5-HT2A receptors potentiates pain produced by inflammatory mediators. *Neuropharmacology* **1996**, *35* (1), 99−110.
(62) Nishiyama, T. Effects of a 5-HT2A receptor antagonist, sarpogrelate on thermal or inflammatory pain. *European journal of pharmacology* **2005**, *516* (1), 18−22.
(63) Dumotier, B. M.; Urban, L. Preclinical mitigation of 5-HT2B agonism-related cardiac valvulopathy revisited. *Journal of pharmacological and toxicological methods* **2024**, *128*, No. 107542.
(64) Rothman, R. B.; Baumann, M. H.; Savage, J. E.; Rauser, L.; McBride, A.; Hufeisen, S. J.; Roth, B. L. Evidence for possible involvement of 5-HT2B receptors in the cardiac valvulopathy associated with fenfluramine and other serotonergic medications. *Circulation* **2000**, *102* (23), 2836−2841.
(65) Watson, J.; Wright, S.; Lucas, A.; Clarke, K. L.; Viggers, J.; Cheetham, S.; Jeffrey, P.; Porter, R.; Read, K. D. Receptor occupancy and brain free fraction. *Drug metabolism and disposition* **2009**, *37* (4), 753−760.
(66) Liu, X.; Smith, B. J.; Chen, C.; Callegari, E.; Becker, S. L.; Chen, X.; Cianfrogna, J.; Doran, A. C.; Doran, S. D.; Gibbs, J. P.; Hosea, N.; Liu, J.; Nelson, F. R.; Szewc, M. A.; Van Deusen, J. Evaluation of cerebrospinal fluid concentration and plasma free concentration as a surrogate measurement for brain free concentration. *Drug Metab. Disposition* **2006**, *34* (9), 1443−1447.
(67) Takamatsu, Y.; Yamamoto, H.; Hagino, Y.; Markou, A.; Ikeda, K. The selective serotonin reuptake inhibitor paroxetine, but not fluvoxamine, decreases methamphetamine conditioned place preference in mice. *Current Neuropharmacology* **2011**, *9* (1), 68−72.
(68) Subhan, F.; Deslandes, P. N.; Pache, D. M.; Sewell, R. D. Do antidepressants affect motivation in conditioned place preference? *European Journal of pharmacology* **2000**, *408* (3), 257−263.

https://doi.org/10.1021/acs.jmedchem.5c03810
J. Med. Chem. 2026, 69, 6210−6229

(69) Fukui, M.; Rodriguiz, R. M.; Zhou, J.; Jiang, S. X.; Phillips, L. E.; Caron, M. G.; Wetsel, W. C. Vmat2 heterozygous mutant mice display a depressive-like phenotype. *J. Neurosci.* **2007**, *27* (39), 10520−10529.
(70) Charney, D. S.; Heninger, G. R.; Sternberg, D. E. Alpha-2 adrenergic receptor sensitivity and the mechanism of action of antidepressant therapy: The effect of long-term amitriptyline treatment. *British Journal of Psychiatry* **1983**, *142* (3), 265−275.
(71) Cichońska, A.; Ravikumar, B.; Rahman, R. AI for targeted polypharmacology: The next frontier in drug discovery. *Curr. Opin. Struct. Biol.* **2024**, *84*, No. 102771.
(72) Abdelsayed, M. AI-driven polypharmacology in small-molecule drug discovery. *International Journal of Molecular Sciences* **2025**, *26* (14), 6996.
(73) Chua, H. E.; Bhowmick, S. S.; Tucker-Kellogg, L. Synergistic target combination prediction from curated signaling networks: Machine learning meets systems biology and pharmacology. *Methods* **2017**, *129*, 60−80.
(74) Awale, M.; Reymond, J.-L. Polypharmacology browser PPB2: target prediction combining nearest neighbors with machine learning. *J. Chem. Inf. Model.* **2019**, *59* (1), 10−17.
(75) Chaudhari, R.; Fong, L. W.; Tan, Z.; Huang, B.; Zhang, S. An up-to-date overview of computational polypharmacology in modern drug discovery. *Expert opinion on drug discovery* **2020**, *15* (9), 1025−1044.
(76) Ferrari, A. M.; Wei, B. Q.; Costantino, L.; Shoichet, B. K. Soft docking and multiple receptor conformations in virtual screening. *Journal of medicinal chemistry* **2004**, *47* (21), 5076−5084.
(77) Gorgulla, C.; Boeszoermenyi, A.; Wang, Z. F.; Fischer, P. D.; Coote, P. W.; Padmanabha Das, K. M.; Malets, Y. S.; Radchenko, D. S.; Moroz, Y. S.; Scott, D. A.; Fackeldey, K.; Hoffmann, M.; Iavniuk, I.; Wagner, G.; Arthanari, H. An open-source drug discovery platform enables ultra-large virtual screens. *Nature* **2020**, *580* (7805), 663−668.
(78) Wu, Y.; Brooks, C. L., III Flexible CDOCKER: hybrid searching algorithm and scoring function with side chain conformational entropy. *J. Chem. Inf. Model.* **2021**, *61* (11), 5535−5549.
(79) Waterborg, J. H.; Matthews, H. R. The Lowry method for protein quantitation. *Basic protein and peptide protocols* **1994**, *32*, 1−4.
(80) Olson, B. J. S. C.; Markwell, J. Assays for determination of protein concentration. *Current protocols in pharmacology* **2007**, *38* (1), A. 3A. 1-A−3A. 29.
(81) Huang, W.; Manglik, A.; Venkatakrishnan, A. J.; Laeremans, T.; Feinberg, E. N.; Sanborn, A. L.; Kato, H. E.; Livingston, K. E.; Thorsen, T. S.; Kling, R. C.; Granier, S.; Gmeiner, P.; Husbands, S. M.; Traynor, J. R.; Weis, W. I.; Steyaert, J.; Dror, R. O.; Kobilka, B. K. Structural insights into μ-opioid receptor activation. *Nature* **2015**, *524* (7565), 315−321.
(82) Maeda, S.; Koehl, A.; Matile, H.; Hu, H.; Hilger, D.; Schertler, G. F. X.; Manglik, A.; Skiniotis, G.; Dawson, R. J. P.; Kobilka, B. K. Development of an antibody fragment that stabilizes GPCR/G-protein complexes. *Nat. Commun.* **2018**, *9* (1), 3712.
(83) Nasr, M. L.; Baptista, D.; Strauss, M.; Sun, Z. Y. J.; Grigoriu, S.; Huser, S.; Plückthun, A.; Hagn, F.; Walz, T.; Hogle, J. M.; Wagner, G. Covalently circularized nanodiscs for studying membrane proteins and viral entry. *Nat. Methods* **2017**, *14* (1), 49−52.
(84) Alvaro, C. G.; Braz, J. M.; Bernstein, M.; Hamel, K. A.; Craik, V.; Yamanaka, H.; Basbaum, A. I. Hippocalcin-like 4, a neural calcium sensor, has a limited contribution to pain and itch processing. *PLoS One* **2020**, *15* (2), No. e0226289.
(85) Chaplan, S. R.; Bach, F. W.; Pogrel, J.; Chung, J.; Yaksh, T. Quantitative assessment of tactile allodynia in the rat paw. *Journal of neuroscience methods* **1994**, *53* (1), 55−63.
(86) Cao, Y. Q.; Mantyh, P. W.; Carlson, E. J.; Gillespie, A.-M.; Epstein, C. J.; Basbaum, A. I. Primary afferent tachykinins are required to experience moderate to intense pain. *Nature* **1998**, *392* (6674), 390−394.
(87) Dwyer, J. M.; Rizzo, S. J. S.; Neal, S. J.; Lin, Q.; Jow, F.; Arias, R. L.; Rosenzweig-Lipson, S.; Dunlop, J.; Beyer, C. E. Acid sensing ion channel (ASIC) inhibitors exhibit anxiolytic-like activity in preclinical pharmacological models. *Psychopharmacology* **2009**, *203* (1), 41−52.

https://doi.org/10.1021/acs.jmedchem.5c03810
J. Med. Chem. 2026, 69, 6210−6229